Article

Cell Host & Microbe

Trivalent RING Assembly on Retroviral Capsids Activates TRIM5 Ubiquitination and Innate Immune Signaling

Graphical Abstract

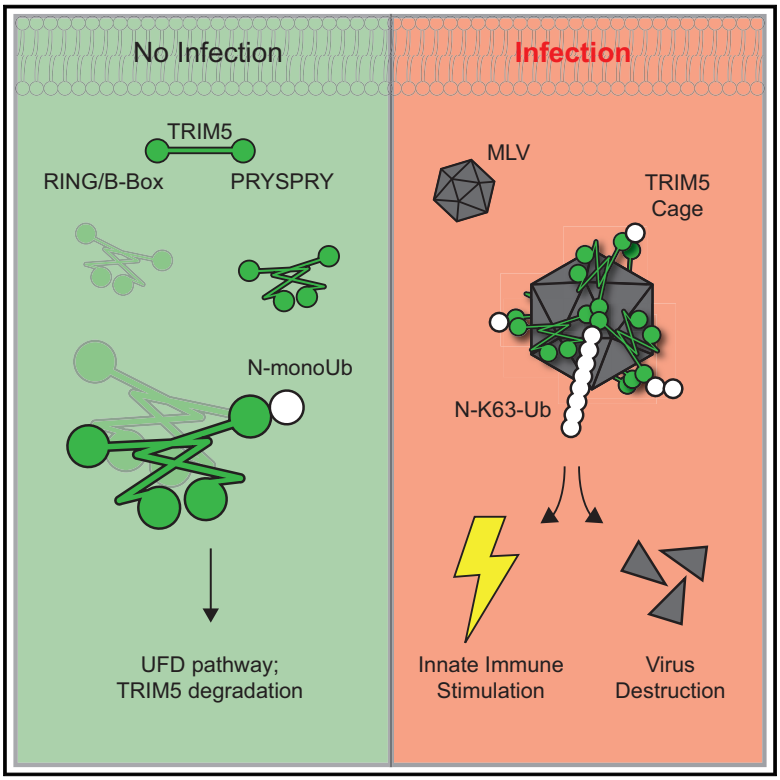

Highlights

- Ubiquitin is redundant for TRIM5 inhibition of viral infection
- TRIM5 assembly drives formation of K63-Ub chains anchored to TRIM5 N terminus
- Three RING domains are necessary for N-terminal K63-Ub extension
- Anchored K63-Ub couples capsid binding with signaling and proteasome recruitment

Authors

Adam J. Fletcher, Marina Vaysburd, Sarah Maslen, Jingwei Zeng, J. Mark Skehel, Greg J. Towers, Leo C. James

Correspondence

lcj@mrc-lmb.cam.ac.uk

In Brief

TRIM5 self-assembles into a lattice that envelopes retroviral capsids, stimulating virion destruction and innate immune signaling. Fletcher et al. demonstrate that self-assembly induces K63-linked ubiquitination (K63-Ub) of the TRIM5 N terminus that drives innate immune stimulation and degradation. Thus, ordered capsid binding allows TRIM5 to couple virus recognition with antiviral responses.

Fletcher et al., 2018, Cell Host & Microbe *24*, 1–15
December 12, 2018
https://doi.org/10.1016/j.chom.2018.10.007

CellPress

Please cite this article in press as: Fletcher et al., Trivalent RING Assembly on Retroviral Capsids Activates TRIM5 Ubiquitination and Innate Immune Signaling, Cell Host & Microbe (2018), https://doi.org/10.1016/j.chom.2018.10.007

Cell Host & Microbe
Article

Trivalent RING Assembly on Retroviral Capsids Activates TRIM5 Ubiquitination and Innate Immune Signaling

Adam J. Fletcher,[1] Marina Vaysburd,[1] Sarah Maslen,[1] Jingwei Zeng,[1] J. Mark Skehel,[1] Greg J. Towers,[2] and Leo C. James[1,3,*]
[1]MRC Laboratory of Molecular Biology, Francis Crick Avenue, Cambridge CB2 0QH, UK
[2]Infection and Immunity, University College London, Cruciform Building, 90 Gower Street, London WC1E 6BT, UK
[3]Lead Contact
*Correspondence: lcj@mrc-lmb.cam.ac.uk
https://doi.org/10.1016/j.chom.2018.10.007

SUMMARY

TRIM5 is a RING domain E3 ubiquitin ligase with potent antiretroviral function. TRIM5 assembles into a hexagonal lattice on retroviral capsids, causing envelopment of the infectious core. Concomitantly, TRIM5 initiates innate immune signaling and orchestrates disassembly of the viral particle, yet how these antiviral responses are regulated by capsid recognition is unclear. We show that hexagonal assembly triggers N-terminal polyubiquitination of TRIM5 that collectively drives antiviral responses. In uninfected cells, N-terminal monoubiquitination triggers nonproductive TRIM5 turnover. Upon TRIM5 assembly on virus, a trivalent RING arrangement allows elongation of N-terminally anchored K63-linked ubiquitin chains (N-K63-Ub). N-K63-Ub drives TRIM5 innate immune stimulation and proteasomal degradation. Inducing ubiquitination before TRIM5 assembly triggers premature degradation and ablates antiviral restriction. Conversely, driving N-K63 ubiquitination after TRIM5 assembly enhances innate immune signaling. Thus, the hexagonal geometry of TRIM5's antiviral lattice converts a capsid-binding protein into a multifunctional antiviral platform.

INTRODUCTION

TRIM proteins, identified by their N-terminal tripartite motif (TRIM; one RING domain, one or two B-Box domains, and a coiled-coil [CC]) constitute the largest family of RING E3 ubiquitin (Ub) ligases in mammals (Han et al., 2011). Many TRIMs have key immune functions, exemplified by TRIM5, which detects and inhibits retroviruses like HIV-1 (Stremlau et al., 2004). TRIM5 self-assembles into hexagonal sheets that "cage" retroviral capsids (Ganser-Pornillos et al., 2011; Li et al., 2016). There are two levels of TRIM5 self-association. First, TRIM5 forms antiparallel homodimers via the CC, with the RING and B-Box domains of paired molecules held apart by ~170 Å (Goldstone et al., 2014; Sanchez et al., 2014; Wagner et al., 2016). Second, each B-Box2 domain forms homotrimers, meaning one TRIM5 dimer forms an edge of the hexagon subunit of the lattice (Figure S6A) (Ganser-Pornillos et al., 2011; Goldstone et al., 2014; Li et al., 2016). TRIM5 oligomerization is critical for antiviral activity because the C-terminal PRYSPRY domain, the region of TRIM5 that binds retroviral capsid, has low affinity for capsid, which is enhanced through avidity (Li and Sodroski, 2008; Li et al., 2016). Higher-order structures formed by TRIM5 are sometimes referred to as cytoplasmic bodies (CBs) and can be provoked in the absence of infection (Diaz-Griffero et al., 2006). However, many aspects of these structures remain poorly understood; for instance, the purpose of localizing three RING domains at each threefold vertex of the lattice. One theory is that this promotes their dimerization and Ub ligase activity (Sanchez et al., 2016; Yudina et al., 2015), but this does not explain the symmetry mismatch. Whether this mismatch is simply a compromise of virus binding, or serves some specific purpose, is currently unclear.

There are two additional outcomes of TRIM5 viral recognition: the generation of an antiviral state (Pertel et al., 2011) and virus destruction by proteasome recruitment (Kutluay et al., 2013; Wu et al., 2006). The latter phenomenon occurs soon after the virus enters the cytoplasm, before viral DNA (vDNA) is transcribed (Stremlau et al., 2004). Both of these processes involve Ub (Campbell et al., 2015; Fletcher et al., 2015; Pertel et al., 2011), whereas mounting evidence suggests that Ub is not required for viral caging and restriction. For example, strong inhibition of viral infection is maintained by RING-less TRIM5 deletion mutants (Diaz-Griffero et al., 2006) and in cells depleted of TRIM5's cognate E2 enzymes where TRIM5 autoubiquitination is impaired (Campbell et al., 2015; Fletcher et al., 2015). One possibility is that ubiquitination occurs upon virus recognition, which triggers downstream effector function. The question of how TRIM5 immune stimulation is activated upon recognition of an incoming retrovirus remains unresolved.

Here we show that TRIM5 builds a K63-Ub chain from its own N terminus following self-assembly. A dynamic trimer of RING domains is required to generate this modification. K63-Ub triggers both immune signaling and degradation by proteasomes. Our data suggest that the specific hexagonal geometry of the TRIM5 lattice serves not only to enable virus binding but also to coordinate immune signaling with pathogen recognition.

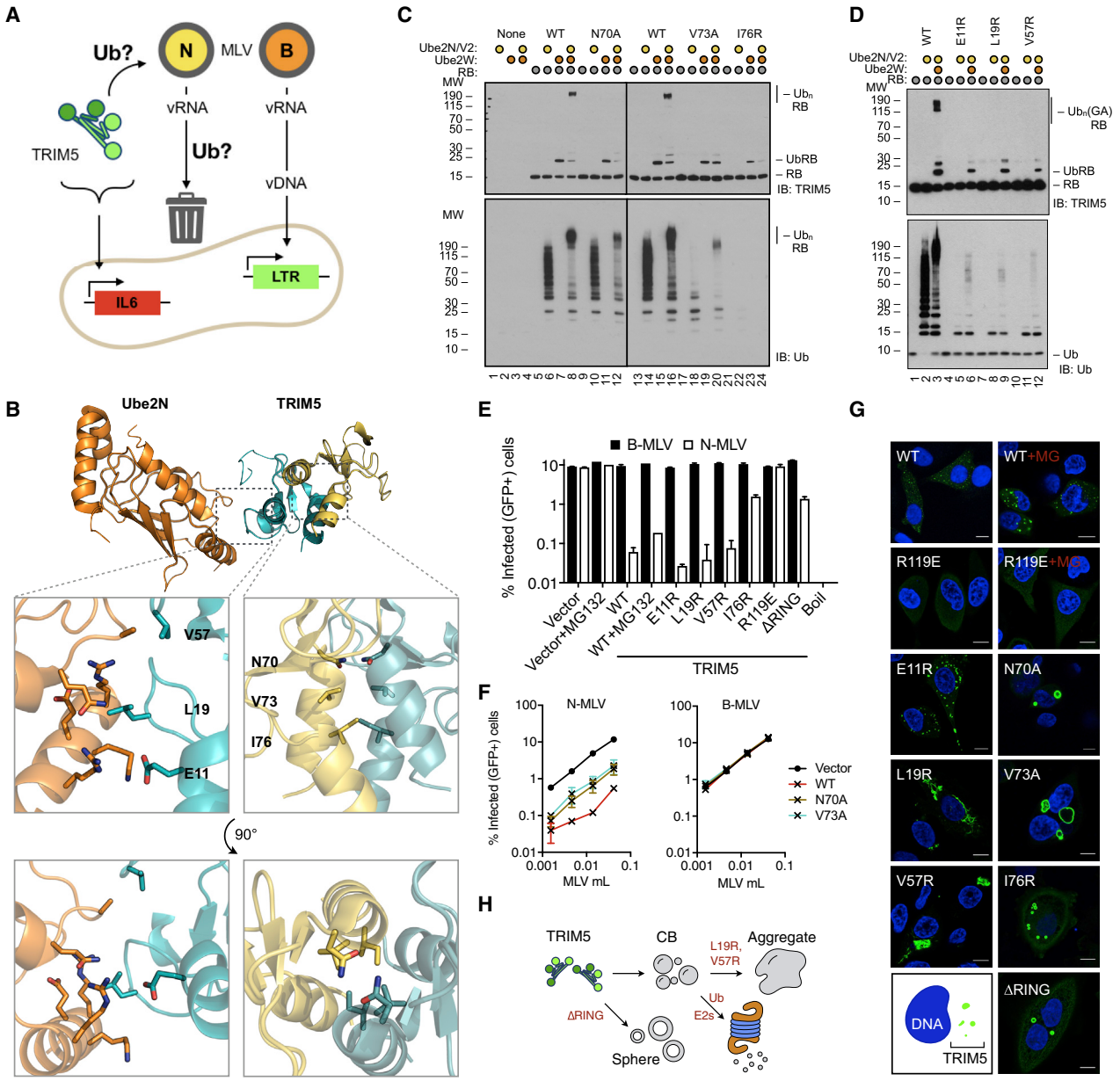

Figure 1. Ubiquitination Is Redundant for Overall Viral Restriction

(A) B-MLV reverse transcribes its genome and integrates into the host. N-MLV recruits TRIM5, is disassembled, and cannot reverse transcribe. TRIM5 stimulates intracellular signaling and transcriptional upregulation of antiviral genes. The timing of Ub during restriction is contested.

(B) Structure of the rhesus macaque TRIM5 RING dimer in complex with Ube2N (2N) (PDB: 4TKP).

(C and D) *In vitro* ubiquitination experiments between TRIM5 RING-B-Box (RB) mutants and Ube2W (C), Ube2N/Ube2V2 (2N/V2) (C and D) or both Ube2W and 2N/V2 (C and D), detecting TRIM5 or Ub.

(E and F) CrFK cells expressing vector or full-length TRIM5 mutants (bearing C-terminal hemagglutinin [HA] tags), infected with N-MLV- or B-MLV-GFP vectors. Percentage infection quantified by flow cytometry (E and F). Boiled virus served as a negative control (E).

(G) Representative confocal fluorescence images of CrFK cells from (E) and (F), detecting HA tag or DNA.

(H) Model. The RING domain determines the morphology and restriction potency, but not the formation, of TRIM5 assemblies.

All experiments representative of at least triplicates. In (E) and (F), error bars represent SD; values are means ± SD.

RESULTS

We began by comprehensively perturbing TRIM5 E3 ligase function, as conflicting data regarding the role of Ub in TRIM5 restriction activity have emerged (Campbell et al., 2015; Fletcher et al., 2015; Pertel et al., 2011; Roa et al., 2012; Wu et al., 2006; Yudina et al., 2015) (Figure 1A). We introduced structure-guided mutations at three positions in the human TRIM5 RING dimer interface (N70A, V73A, I76R) and three positions at the RING-E2 enzyme interface (E11R, L19R, V57R) (Figure 1B). We made recombinant

human TRIM5 proteins comprising the RING and B-Box2 domains (RBs). In solution, RB was in dynamic monomer-dimer equilibrium; dimer interface mutants were more monomeric (Figure S1A). We tested each RING mutants' ubiquitination activity *in vitro* with cognate E2s Ube2W (2W) and Ube2N/Ube2V2 (2N/V2), which build anchored K63-polyUb chains (K63-Ub) on TRIM5 (Fletcher et al., 2015). Wild-type (WT) TRIM5 RBs produced unanchored Ub chains of heterogeneous lengths with 2N/V2 alone (Figure 1C, lane 6), and a high molecular weight (Mw), more homogeneous length anchored chain with 2N/V2 and 2W (Figure 1C, lane 8). Monoubiquitinated RB was generated with 2W alone (Figure 1C, lane 7). The RING dimer mutants were all strongly impaired in anchored chain elongation and reduced for monoubiquitin (monoUb). I76R and V73A, but not N70A, were also impaired for free chain synthesis, suggesting that mechanisms of chain extension from free or anchored Ub are distinct (Figure 1C). Each E2 interface mutant was severely disabled in the synthesis of both kinds of polyUb (Figure 1D), and E11R and V57R were also reduced for monoUb (Figure S1B). Overall, anchored K63-Ub synthesis was very sensitive to mutation of either the RING dimer or E2 interfaces.

To determine how these alterations affect antiviral function, we expressed full-length human TRIM5 mutants in permissive feline CrFK cells and infected them with TRIM5-sensitive N-tropic murine leukemia virus (N-MLV) or TRIM5-insensitive B-MLV retroviral vectors carrying a GFP reporter gene. The E2 interface mutants E11R, L19R, and V57R maintained WT levels of antiviral activity (Figure 1E) despite not producing any polyUb *in vitro*. The RING dimer interface mutants suffered a partial loss in antiviral activity but retained the ability to restrict N-MLV infection by 10-fold (Figures 1E and 1F), despite N70A retaining free chain synthesis activity *in vitro* where V73A had lost it (Figure 1B). Therefore, the partial loss of restriction activity by the RING dimer interface mutants is more consistent with a structural contribution made by the RING dimer to the restrictive lattice (Li et al., 2016; Wagner et al., 2016). To test this, we deleted the RING domain entirely and assessed its restriction activity in parallel. As expected, loss of the RING domain only caused a partial loss of restriction; 10-fold inhibition of infection remained (Figure 1E). Conversely, the B-Box self-association mutant R119E was completely unable to restrict infection (Figure 1E) (Diaz-Griffero et al., 2007), confirming that higher-order assembly, but not ubiquitination, is required for TRIM5's restriction activity.

TRIM5 self-assembly is shown by the formation of dynamic puncta called CBs. MG132 slows TRIM5 degradation and augments CB size (Figure 1G) (Campbell et al., 2008). TRIM5 B-Box mutant R119E does not self-associate (Wagner et al., 2016) or form CBs (Diaz-Griffero et al., 2007) even after MG132 treatment (Figure 1G), consistent with its failure to restrict infection (Figure 1E). However, each RING mutant formed subcellular structures, even in the absence of MG132, consistent with effective self-association and potent antiviral activity (Figure 1G). Notably, although mutant E11R formed regular CB like WT (Figure 1G), mutants L19R and V57R formed larger structures (Figures 1G and 1H), which we predict are derived from CBs that have grown due to impaired disassembly (see below). In contrast, the ΔRING and dimer mutants formed hollow spheres (Figures 1G and 1H), consistent with the RING dimer making a structural contribution to the restrictive lattice (Figure 1E). Thus, interfering with TRIM5 ubiquitination affects CB growth and persistence, suggesting ubiquitination plays a crucial role in disassembly of the TRIM5 platform.

TRIM5 has a proteasome-dependent short half-life in cells (Diaz-Griffero et al., 2006). Cycloheximide chase experiments revealed that each of the six RING mutants failed to turn over effectively (Figures 2A and 2B; compare with WT in the presence of MG132; Figure S2A), agreeing with exaggerated assembly phenotypes (Figure 1). Turnover of E11R was reduced but not abolished, consistent with the WT-like CB that this mutant formed (Figure 1G). TRIM5 turnover was also abolished if self-association was prevented by mutation R119E (Figure S2B) (Li and Sodroski, 2008), suggesting TRIM5 self-association is required to bring RING domains together, recruit E2s, and initiate Ub-dependent turnover.

TRIM5-mediated virus disassembly occurs soon after virus entry and causes an inhibition of vDNA synthesis (Kutluay et al., 2013; Stremlau et al., 2004), which thus serves as a quantitative assay for virus disassembly (Roa et al., 2012). Proteasome inhibition, in addition to preventing TRIM5 turnover (Figure S2A) (Diaz-Griffero et al., 2006; Rold and Aiken, 2008), selectively restores vDNA synthesis but not infection (Wu et al., 2006). We infected CrFK expressing empty vector, WT, E11R, L19R, V57R, I76R, R119E, or ΔRING TRIM5, with N- or B-MLV and measured the level of vDNA at 6 hr post-infection. Vector and WT TRIM5 expressing cells were additionally treated with MG132. As expected, WT TRIM5 potently reduced the levels of vDNA; MG132 treatment, or RING deletion, restored vDNA synthesis (Figure 2C), but not viral infection (Figure 1E). R119E was completely inactive, as expected. RING mutants L19R, V57R, and I76R were also unable to inhibit vDNA synthesis, consistent with a failure to recruit proteasomes via Ub chain formation. The E11R mutant retained weak restriction of vDNA synthesis consistent with reduced, but not abolished, turnover (Figure 2A). To confirm the pathway was conserved in human cells, we also deleted TRIM5 by CRISPR/Cas9 in TE671 cells, then reconstituted with WT, L19R, or R119E mutant TRIM5. As in CrFK, only WT TRIM5 conferred a potent block to N-MLV vDNA synthesis (Figures 2D and S2C), while both WT and L19R TRIM5 conferred potent restriction of viral infection (Figure 2E). Therefore, affecting TRIM5 ubiquitination in both feline and human cells impairs virus disassembly but not viral restriction.

To correlate ubiquitination specificity *in vitro* and in cells, we probed TRIM5 assemblies for Ub. Using a linkage-specific antibody, we found that WT CBs were rich in K63-Ub; 96% of CBs were K63-Ub positive (Figure 2F). In contrast, 16%, 2%, and 5% of the assemblies formed by RING mutants E11R, L19R, and I76R, respectively, were labeled with K63-Ub (Figure 2F). Thus, RING mutants with ubiquitination defects *in vitro* (Figure 1) are unable to turn over, inhibit vDNA synthesis, or catalyze K63-Ub formation in cells. These data are consistent with a model in which TRIM5 undergoes self-association, autoubiquitinates, recruits proteasomes, and disassembles viral cores before significant vDNA synthesis occurs. However, this model assumes that TRIM5 autoubiquitination drives its own destruction at the proteasome, with premature virus disassembly (and degradation) an antiviral by-product. To understand whether TRIM5 RING-dependent K63-Ub synthesis can drive proteasome-dependent

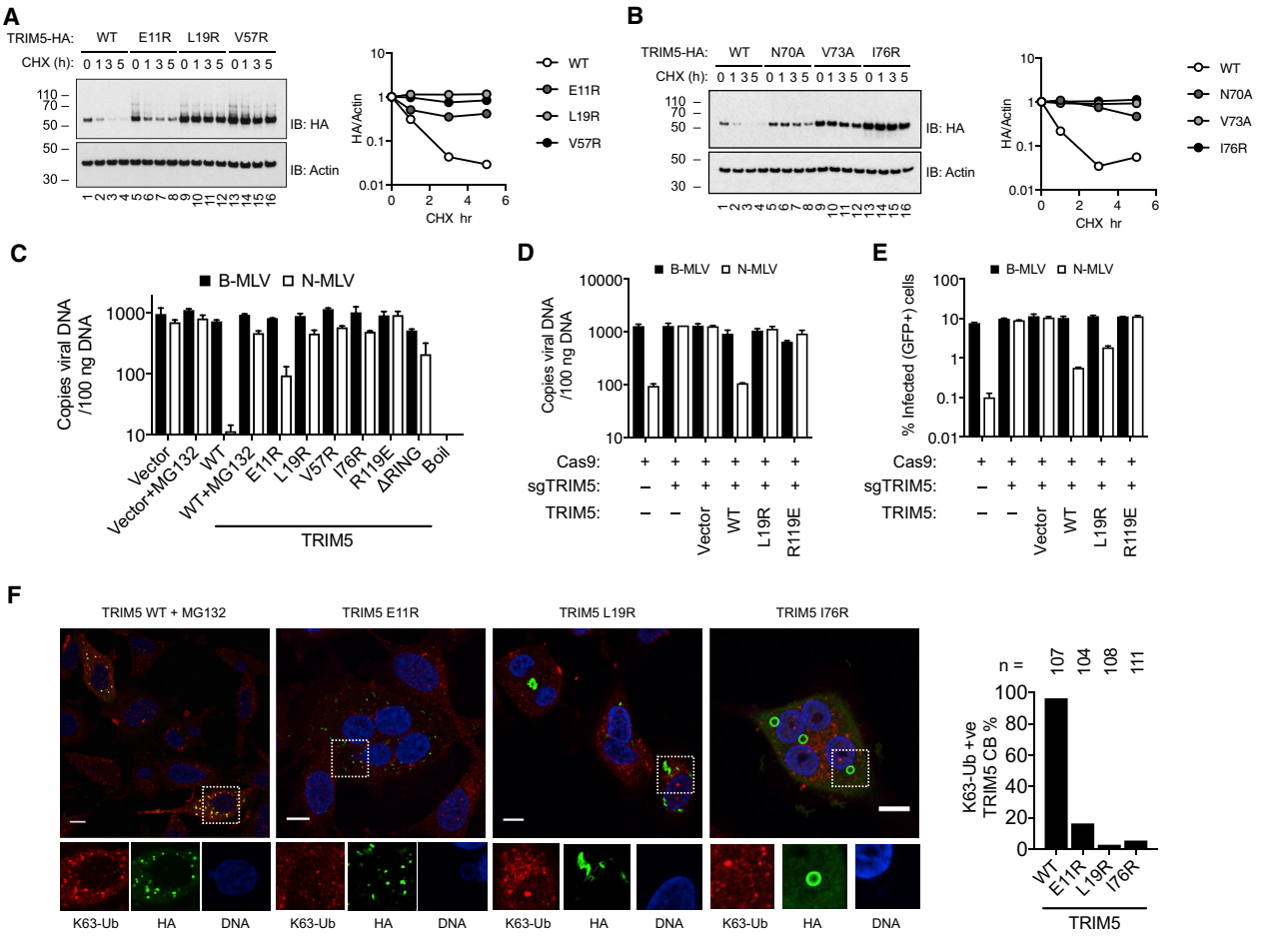

Figure 2. Ubiquitination Drives TRIM5 Turnover and Virus Destruction

(A and B) Left: cycloheximide (CHX) chase experiments of CrFK cells expressing full-length TRIM5 E2 interface mutants (A) or TRIM5 RING dimer mutants (B), bearing C-terminal HA tags (A and B). Immunoblots detecting HA tag or β-actin. Right: densitometry of immunoblots shown.

(C and D) CrFK cells (C) or TE671 cells transduced with Cas9 and TRIM5-specific single guide RNA (D) and expressing empty vector or full-length TRIM5 mutants (bearing C-terminal HA tags), infected with N-MLV- or B-MLV-GFP vectors, viral DNA copies quantified by GFP TaqMan qPCR. In (C), vector or WT TRIM5 cells were also treated with 10 μM MG132. Boiled virus served as a control for plasmid contamination.

(E) TE671 cells from (D) infected with N-MLV-GFP or B-MLV-GFP vectors, percentage infection quantified by flow cytometry.

(F) Representative confocal fluorescence images of CrFK cells expressing full-length TRIM5 mutants (bearing C-terminal HA tags), detecting HA tag, K63-Ub, or DNA. Cells containing K63-Ub-positive CBs were counted and expressed as percentage of total cells counted.

All data are representative of at least two replicates. (C–E) Error bars represent SD. In (F), n = number of cells counted in the experiment shown.

degradation, we required deeper understanding of TRIM5 ubiquitination in cells.

TRIM5 ubiquitination also drives innate immune signaling, but how Ub signaling assimilates with restriction is poorly understood. To investigate this, we first measured innate immune signaling pathways during restriction of N-MLV infection by endogenous TRIM5 in THP-1 cells. We observed transcriptional upregulation of cytokines *IL6*, *IL1B*, *IFNB1*, and *TNFA*, and enzymes *IFIT1*, *NLRP3*, *PTGS2*, and *SOD2*, in response to N-, but not B-MLV (Figure 3A). *PTGS2* and *SOD2* were previously found in a screen for TRIM5-regulated genes in these cells (Pertel et al., 2011). The response was TRIM5 dependent (Figure 3B); TRIM5 depletion by small hairpin RNA was confirmed by rescue of restricted N-MLV infection (Figure 3C). To determine whether immune gene transcription is induced by TRIM5 activation of the NF-κB pathway, we monitored canonical NF-κB signaling by immunoblot and immunofluorescence microscopy during viral infection. This approach revealed a striking phosphorylation of IκBα at serines 32/36 (Figure 3D), and relocation of NF-κB subunit p65 from the cytoplasm to the nucleus (Figure 3E) upon challenge with N-, but not B-MLV. These data confirm that TRIM5 performs pattern recognition during retroviral restriction, resulting in activation of NF-κB and immune gene induction.

Transient TRIM5 overexpression is sufficient to activate NF-κB signaling in the absence of infection and can be detected in luciferase reporter assays (Pertel et al., 2011). We confirmed that such NF-κB signaling also results in cytokine transcription, by measuring upregulated expression of *IL6* and *PTGS2* (Figures 3F and 3G). We hypothesized that enforced TRIM5 assembly in the absence of a viral template drives this phenomenon. B-Box mutant R119E was unable to stimulate NF-κB (Figure 3H) and was significantly less decorated by Ub (Figure 3I),

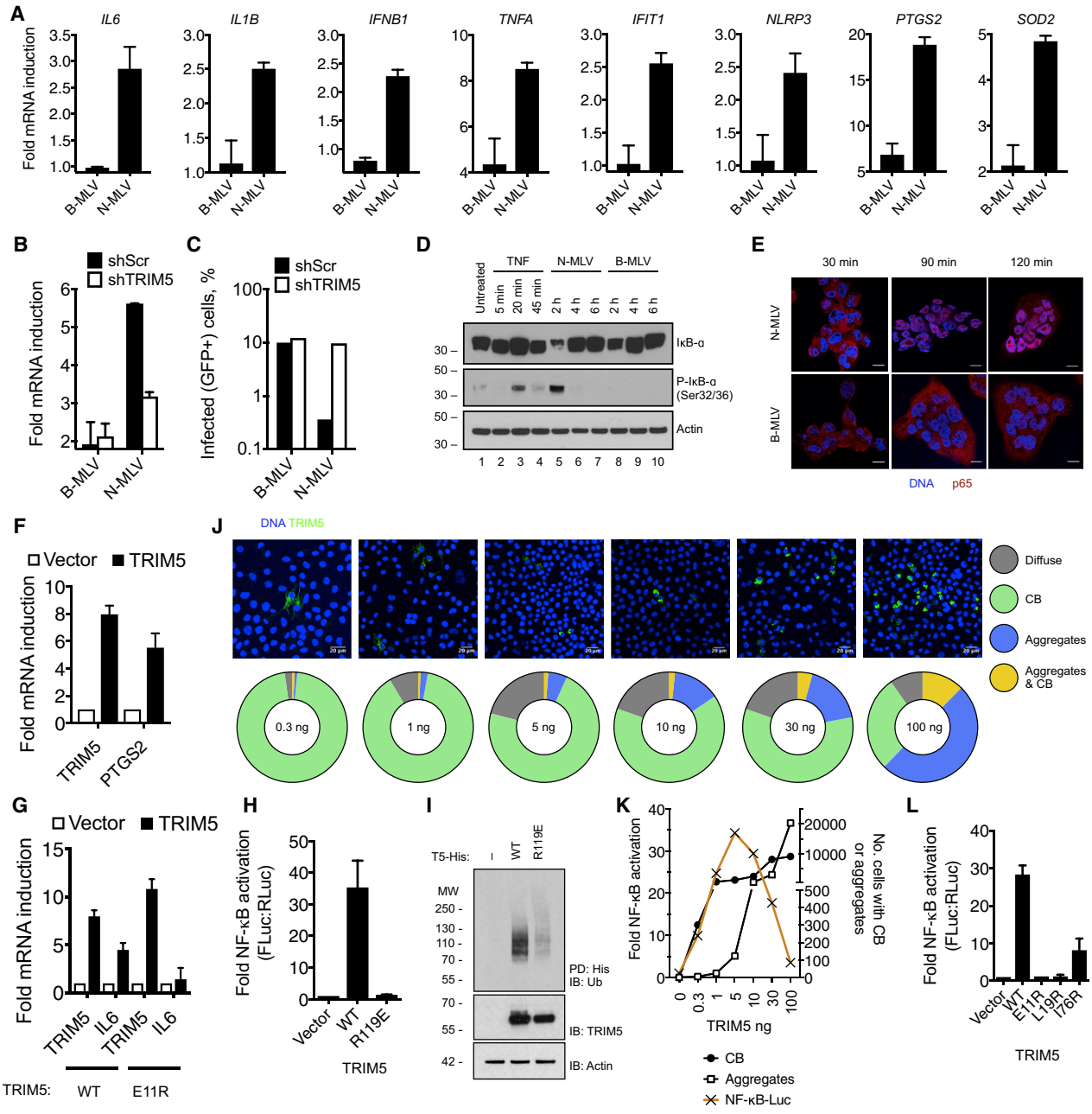

Figure 3. TRIM5 Cytoplasmic Bodies Are Signaling Platforms

(A and B) (A) Differentiated THP-1 cells infected with N- or B-MLV vector, or media alone, and mRNA fold inductions relative to media were quantified (ΔΔCt) by qPCR using *ACTB* as an uninduced control. In (B), THP-1 expressed control (shScr) or TRIM5-specific (shTRIM5) small hairpin RNA (shRNA).

(C) THP-1 from (B) were infected with N- or B-MLV-GFP and percentage infection quantified by flow cytometry.

(D) Differentiated THP-1 cells infected with N- or B-MLV, or 10 ng/mL TNFα, for times indicated. Immunoblots detecting phospho-IκBα, IκBα, and β-actin.

(E) Representative confocal fluorescence images of differentiated THP-1 cells, infected with N- or B-MLV for the times indicated, detecting p65 or DNA.

(F and G) *TRIM5*, *PTGS2* (F), and *IL6* (G) expression relative to *ACTB* in 293T following transfection with WT or E11R (G) TRIM5.

(H) NF-κB-Luc activation in 293T by WT or R119E TRIM5.

(I) Immunoblot of WT or R119E TRIM5-His pull-downs (PDs) from 293T cells, detecting Ub in PD fraction and TRIM5 or β-actin in input fraction.

(J) Representative confocal fluorescence images of 293T transfected with increasing doses of TRIM5 plasmid (bearing C-terminal HA tag), NF-κB-FLuc, and RLuc, detecting HA tag or DNA. Cells classified as containing diffuse TRIM5, CBs, aggregated TRIM5 (aggregates), or aggregates and CBs. Cells counted in eight fields of view, and different cell classes represented as parts of a whole.

(K) NF-κB-FLuc activation in cells from (J), plotted against the number of cells at each plasmid dose containing either CB or aggregates.

(L) NF-κB-Luc activation in 293T by WT, E11R, L19R, or I76R TRIM5.

All data are representative of at least two replicates. All data are mean values; error bars represent SD. See also Figure S3.

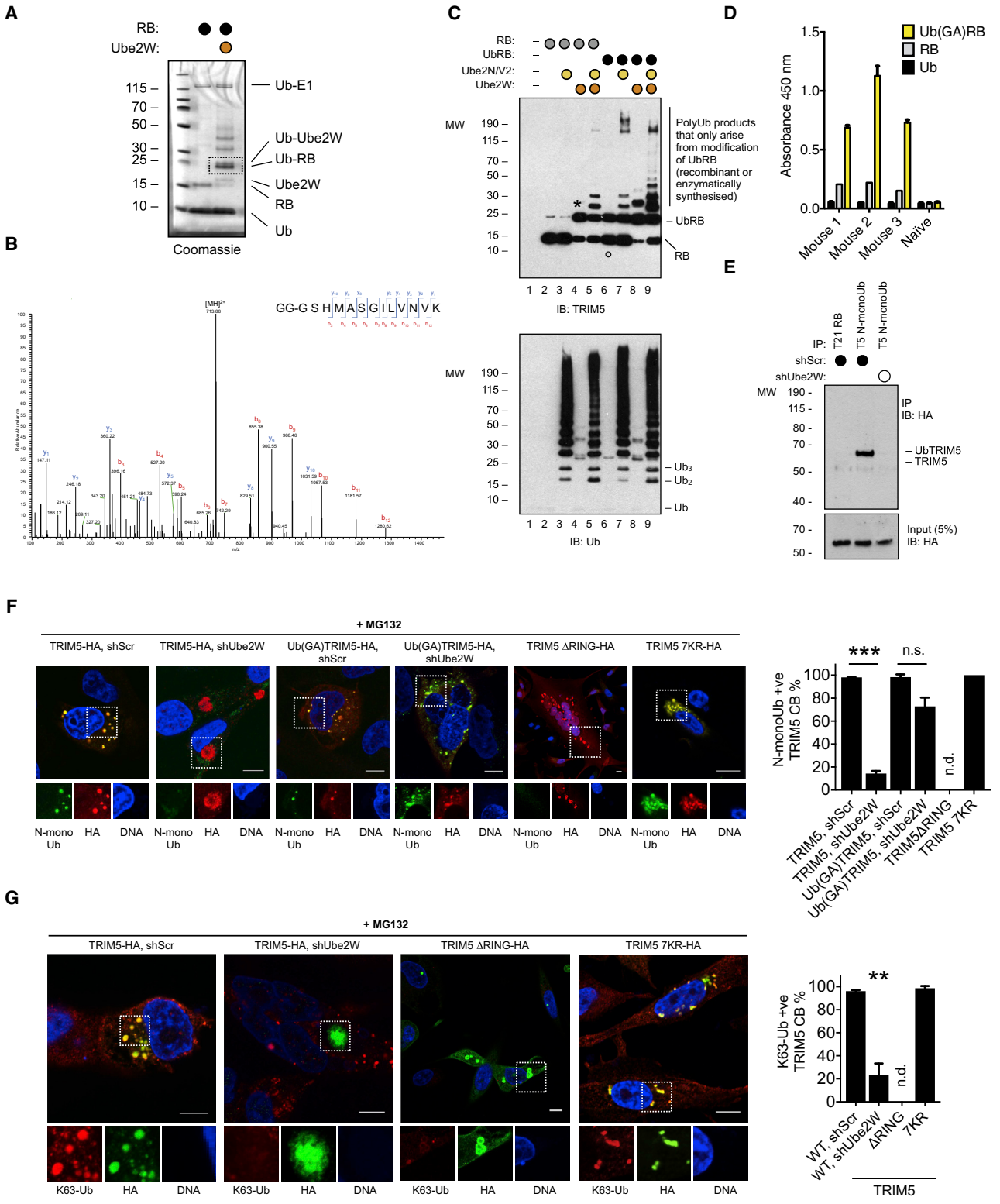

Figure 4. TRIM5 CBs Harbor N-Terminal Ub

(A) Coomassie gel of *in vitro* reaction between 2W and TRIM5 RB. Dotted box indicates region excised for LC-MS/MS.

(B) Tandem mass spectrometry spectra of the N-terminal diGly-modified N-terminal peptide identified in (A).

(C) Immunoblots of *in vitro* ubiquitination reactions between UbRB, 2W, and 2N/V2, detecting TRIM5 (top) and Ub (bottom). Circle indicates free RB protein co-purified with UbRB; asterisk indicates enzymatically synthesized UbRB.

(legend continued on next page)

supporting a relationship between self-association, catalytic activation, autoubiquitination, and signaling. To further explore the correlation, we measured NF-κB activation and CB frequency upon titration of transfected TRIM5 plasmid in 293T cells. At low TRIM5 levels, the protein formed numerous micrometer-sized CBs per cell and both CB formation and NF-κB stimulation increased with plasmid dose (Figures 3J, 3K, S3A, and S3B). At plasmid doses above 5 ng, NF-κB stimulation declined, despite a steady increase in the number of CB-containing cells. However, the reduction in NF-κB signaling was accompanied by a rising frequency of TRIM5 aggregates (Figures 3J, 3K, S3A, and S3B), which closely resembled the aggregates formed by E2 binding mutants L19R and V57R (Figure 1G). NF-κB output was greatest when CB numbers were high and aggregate numbers low (Figure 3K). We hypothesize that the discrete CBs, which localize around virus during restriction (Campbell et al., 2008), contain enzymatically active TRIM5. In contrast, the large aggregates contain inactive TRIM5 and repress signaling through protein misfolding or sequestration. As TRIM5 expression increases and drives self-assembly, first functional CBs form and then larger non-functional aggregates accumulate, explaining the bell-shaped response curve. We observed equivalent bell-shaped NF-κB stimulation profiles by TRIM1, TRIM32, and TRIM38 (Figure S3C), whereas IKK2 stimulation of NF-κB was not self-limiting and increased exponentially with dose (Figure S3C). TRIM5 RING-E2 interface mutants E11R, L19R, and I76R (restriction proficient but ubiquitination deficient in cells and *in vitro*; Figure 1) were defective for NF-κB activation (Figures 3G and 3L), despite forming discrete cytoplasmic puncta (Figure S3D). Thus, these mutants separate ubiquitination from antiviral activity, and antiviral activity from innate immune signaling. TRIM5 self-association drives inflammatory polyUb synthesis, suggesting CBs and the restrictive lattice are signaling platforms.

To investigate which Ub species form within inflammatory CBs, we first sought evidence for monoUb. Depletion of 2N/V2 in cells reveals a 2W-dependent TRIM5 species bearing a single Ub (Fletcher et al., 2015), suggesting a single site of Ub conjugation. 2W has a specialized active site and flexible C-terminal region, which collectively favor ubiquitination of N-terminal over lysine amines (Tatham et al., 2013; Vittal et al., 2015). However, mass spectrometry has not detected authentic N-terminal ubiquitinated peptides in cells, making the existence of this modification and its functional significance difficult to study. To determine whether TRIM5 is labeled at its N terminus in CBs, we therefore adopted a combined *in vitro* and cellular approach. We first confirmed that 2W targets the TRIM5 N terminus *in vitro*. The RB proteins we used had non-acetylated N termini and seven available lysine residues. Upon incubation with 2W, we observed robust auto-monoubiquitination, shown by depletion of the RB band and appearance of a band corresponding with monoUb-RB (Figure 4A). Discrete higher-Mw bands were also observed in Coomassie gels (Figure 4A), suggesting monoubiquitination of 2W also occurs (Tatham et al., 2013), as well as secondary monoubiquitination on RB lysine residues once the N terminus has been conjugated (Fletcher et al., 2015; Vittal et al., 2015), as suggested by western blots for TRIM5 (Figure S1B). However, mass spectrometric analysis of the excised monoUb-RB band confirmed that the predominant Ub conjugation had occurred exclusively at the RB N terminus; only N-terminal diGly-modified, but not lysine-modified diGly, peptides were detected (Figure 4B). To determine whether N-terminal monoUb (N-monoUb) is able to prime anchored K63-Ub synthesis by TRIM5, we made a linear UbRB fusion protein by genetically fusing Ub to the TRIM5 RB N terminus. In the presence of 2N/V2, recombinant UbRB became robustly labeled with anchored polyUb (Figure 4C). Importantly, this activity was now independent of 2W (Figure 4C, compare lanes 3 and 7). Thus, N-monoUb is a primer for TRIM5-anchored K63-Ub (N-K63-Ub).

Previously, we detected acetylated TRIM5 N termini by mass spectrometry, following non-denaturing purification of overexpressed TRIM5 in cells (Fletcher et al., 2015). We re-examined this observation by denaturing cells with guanidine before affinity purification of ectopically expressed TRIM5. Trypsin digests of captured protein were assessed by liquid chromatography-tandem mass spectrometry (LC-MS/MS). While we were unable to identify di-Gly-modified N-terminal peptides, as expected, this approach revealed both acetylated and non-acetylated (demethionylated) N termini, suggesting that the TRIM5 N terminus in cells is not constitutively acetylated (Figure S4A). Knowing 2W can modify non-acetylated TRIM5 N termini (Figures 4A and 4B), we generated N-monoUb-specific antisera by immunizing mice with recombinant UbRB. From here on, we used linear UbRB proteins bearing Gly-Ala substitution at the two final residues of Ub, which prevented deubiquitination in bacteria (Ub(GA)RB) (Figure S4B). Antisera from several mice were highly specific to Ub(GA)RB and poorly recognized either Ub or unmodified RB by ELISA (Figure 4D). To ensure specificity, we depleted RB-reactive antibodies from the serum by incubation on RB-coated plates. The resultant antiserum efficiently immunoprecipitated ectopic TRIM5 from control cells, but not from 2W-depleted cells (Figures 4E and S1C), suggesting that TRIM5 is labeled with N-monoUb in cells. Conversely, immunoprecipitation of full-length ectopic Ub(GA)TRIM5 was insensitive to 2W depletion (Figures S1C and S4C), demonstrating that genetic fusion of N-monoUb to TRIM5 obviates 2W dependence in cells as it had *in vitro* (Figure 4C).

We next used our specific antibodies to determine if N-monoUb occurs within TRIM5 CB. We stably expressed WT or mutant TRIM5 in TE671 cells treated with MG132 to enhance CB visibility (Campbell et al., 2008; Wu et al., 2006). CBs formed by WT TRIM5 were robustly detected by the anti-N-monoUb

(D) ELISA of sera from four mice, one naive and three immunized with recombinant Ub(GA)RB, measuring binding to recombinant Ub, RB, or Ub(GA)RB.
(E) Immunoprecipitation (IP) of TRIM5-HA from TE671 expressing control (shScr) or 2W-specific (sh2W) shRNA, using anti-N-terminal monoubiquitin (T5 N-monoUb) or anti-TRIM21 RING-B-Box (T21 RB) sera, detecting HA tag in IP or input fractions.
(F and G) Representative confocal fluorescence images of TE671 expressing TRIM5 or Ub(GA)TRIM5 (C-terminal HA tag), and shScr or sh2W; or expressing TRIM5ΔRING or TRIM5 7KR (C-terminal HA tag), detecting N-monoUb (F), K63-Ub (G), HA tag, and DNA. Scale bar, 10 μm.
All data are representative of at least duplicates. **Unpaired t test, $p < 0.01$. ***Unpaired t test, $p < 0.001$. n.s., not significant; n.d., not determined. Error bars represent SD. In (F), n = 2, ~100 cells scored per condition per replicate. In (G), n = 2, 40–60 cells scored per condition per replicate.

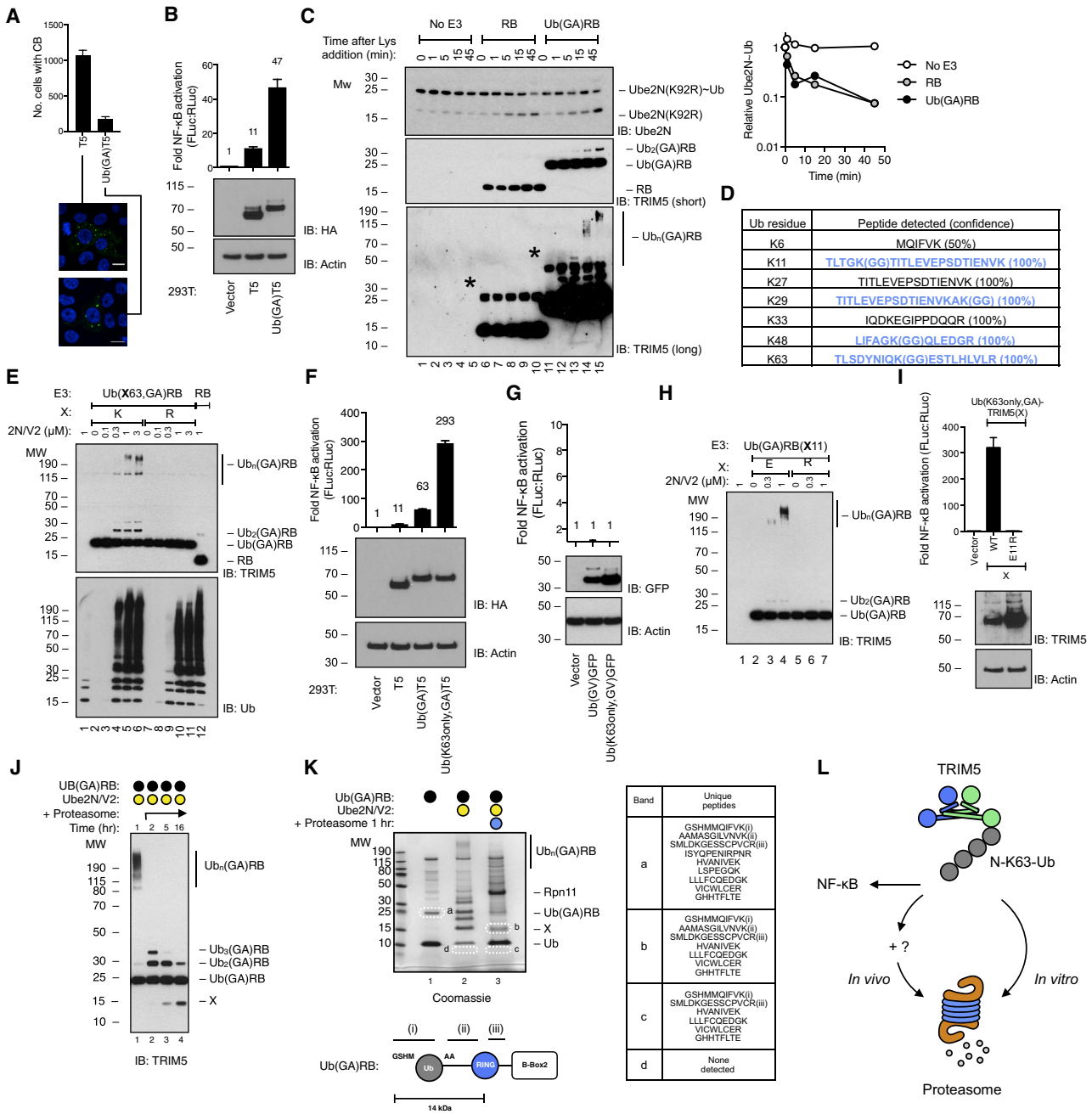

Figure 5. N-Terminal Ub Promotes TRIM5 Immune Signaling, Chain Anchoring, and Proteasomal Degradation

(A) Representative confocal fluorescence images of 293T transfected with TRIM5-HA or Ub(GA)TRIM5-HA, NF-κB-Luc, and RLuc, detecting HA tag or DNA, and frequency of CB-containing cells quantified.

(B) Top: NF-κB-Luc activation in cells from (A). Bottom: immunoblot detecting HA tag and β-actin.

(C) 2N/V2∼Ub discharge experiments with Ube2N(K92R). Left: reactions assessed by immunoblot detecting 2N (top) or TRIM5 (bottom two panels). Asterisk indicates contaminant protein. Right: densitometry of immunoblot shown.

(D) LC-MS/MS analysis of 293T-expressed Ub(GA)TRIM5-His identifies four sites of Ub conjugation in N-monoUb, as inferred by modification of Lys with diGly (GG). Ubiquitinated peptides shown in blue. Peptide confidence in parentheses.

(E) Immunoblot of *in vitro* reactions between TRIM5 RB, Ub(GA)RB, or Ub(K63R,GA)RB and 2N/V2, detecting TRIM5 (top) or Ub (bottom).

(F and G) Top: NF-κB-FLuc activation in 293T by TRIM5 (F) or GFP (G) constructs indicated. Bottom: immunoblot detecting HA tag and β-actin.

(H) Immunoblot of *in vitro* reactions between TRIM5 Ub(GA)RB or Ub(GA)RB(E11R) and 2N/V2, detecting TRIM5.

(I) Top: NF-κB-Luc activation in 293T by constructs indicated. Bottom: immunoblot detecting the HA tag and β-actin.

(J) Immunoblot of *in vitro* reactions between TRIM5 Ub(GA)RB, first conjugated with N-K63-Ub by 2N/V2, and proteasomes, incubated for 1–15 hr, detecting TRIM5.

(legend continued on next page)

serum (Figure 4F). We previously found that 2W can target certain TRIM5 lysine residues *in vitro* when the TRIM5 N terminus was acetylated (Fletcher et al., 2015). However, CBs formed by the TRIM5 7KR mutant, containing Lys-Arg substitutions at the seven positions targeted by 2W and thus refractory to modification at these positions, were also detected by the anti-N-monoUb serum (Figure 4F). Interestingly, 2W depletion increased the frequency of large TRIM5 aggregates that bore hallmarks of aggresomes; mean diameter 9.6 ± 2.2 μm (n = 66), perinuclear and vimentin caged (Figures S1C and S4D) (Johnston et al., 1998). Critically, these TRIM5 aggresomes were invisible to the anti-N-monoUb serum (Figure 4F). Bypassing 2W by genetically installing N-monoUb (Ub(GA)TRIM5) led to N-monoUb-rich CBs regardless of 2W expression (Figure 4F), supporting the model that 2W catalyzes TRIM5 N-monoUb in cells. As expected, spherical assemblies formed by TRIM5ΔRING were invisible to the antiserum (Figure 4F). WT CBs were also labeled with K63-Ub (Figure 4G), which, like N-monoUb, was RING dependent, confirming the ectopic TRIM5 was responsible for ubiquitination (Figure 4G). Importantly, 2W depletion reduced K63-Ub detection to 24% of CBs, suggesting that the majority of the K63-Ub signal comes from Ub chains anchored to TRIM5 by 2W and not unanchored K63-Ub chains (Figure 4G). CBs formed by TRIM5 7KR were also robustly labeled with K63-Ub (Figure 4G), indicating that the 2W-dependent K63-Ub signal was lysine independent. Together, these data suggest that inflammatory CBs are sites of N-K63-Ub synthesis.

We next asked whether N-K63-Ub chains contribute to NF-κB activation. Given that TRIM5 CB frequency was proportional to NF-κB activation at low plasmid dose (Figure 3), we first compared CB formation by full-length WT or Ub(GA)TRIM5 at low-dose expression in 293T cells. No MG132 was used in these transient experiments. Interestingly, although Ub(GA)TRIM5 could undergo self-assembly, its CBs were much less frequent than WT CBs (Figure 5A), suggesting N-monoUb disfavors CB stability. In spite of this, and equivalent protein expression compared with WT, Ub(GA)TRIM5 was substantially more effective at stimulating NF-κB (Figure 5B). N-monoUb did not affect the RING monomer-dimer equilibrium (Figure S5A), indicating it had not enhanced E3 ligase activity per se. Indeed, the RB and Ub(GA)RB proteins were equally effective at stimulating Ub discharge by 2N (Figure 5C). However, Ub(GA)RB uniquely promoted Ub discharge onto itself, despite the fact that the E3 and E2∼Ub were incubated with a vast excess of free Ub and lysine to act as Ub acceptors (E3 at 1.5 μM, Ub at 18 μM, lysine at 50 mM) (Vittal et al., 2015). Thus, N-monoUb favors anchored over free K63-Ub synthesis, revealing a correlation between NF-κB activation and anchored K63-Ub.

Next, we found that the N-monoUb was ubiquitinated at residues K11, K29, K48, and K63 in 293T cells (Figure 5D). *In vitro*, mutation of K63 in N-monoUb abolished anchored, but not free, polyUb synthesis by Ub(GA)TRIM5 (Figure 5E), pinpointing K63 as the sole acceptor lysine for anchored polyUb. We therefore mutated all N-monoUb lysines in full-length Ub(GA)TRIM5 except K63, anticipating this would license functional TRIM5 autoubiquitination (N-K63-Ub) but block signals originating from K11, K29, and K48. Strikingly, this manipulation further enhanced NF-κB activation by TRIM5 in 293T cells (Figure 5F), supporting the notion that N-K63-Ub in CB is inflammatory in nature.

The effect of N-monoUb was TRIM5 specific because non-hydrolyzable Ub(G76V)GFP fusions did not activate NF-κB (Figure 5G). Moreover, RING mutants E11R, L19R, or V57R introduced into Ub(K63only,GA)TRIM5, to prevent all autoubiquitination using 2N/V2 (Figure 5H) eliminated NF-κB activation (Figures 5I and S5B). B-Box mutant R119E also abolished NF-κB activation by this construct (Figure S5B), consistent with a model whereby N-K63-Ub extension only occurs after TRIM5 self-association (see below). I44A, A46E, and G47E mutation of the Ub hydrophobic patch bound by Ube2V2 (Branigan et al., 2015) (Figure S5C) impaired anchored Ub chain extension on Ub(GA)RB *in vitro* (Figure S5D) and NF-κB activation by Ub(K63only,GA)TRIM5 in cells (Figure S5B), confirming that Ube2V2 mediates inflammatory chain extension from N-monoUb. We conclude that N-monoUb fusion bypasses 2W, drives anchored N-K63-Ub synthesis, and augments the NF-κB response.

We next sought to reconstitute TRIM5 degradation *in vitro*. We assembled HMW N-K63-Ub on TRIM5 RB by incubating Ub(GA)RB protein with 2N/V2 (Figure 5J, lane 1) before adding proteasomes purified from TE671 cells (Figure S5E). Proteasomes efficiently removed polyUb from Ub(GA)RB by 1 hr (Figure 5J, lane 2). Longer incubations generated a low-Mw TRIM5 degradation product of 14 kDa (Figure 5J, lanes 3–4). LC-MS/MS analysis of this band (Figure 5K, band b) revealed an abundance of both Ub- and TRIM5-derived peptides (Figure 5K, right). Importantly, all N-terminal Ub peptides bore a GSHM tag, which was present in recombinant Ub(GA)RB but not recombinant Ub (Figure 5K, bottom). This suggests that Ub(GA)RB had been proteolysed within the RING domain, rather than only deubiquitinated. Supporting this, LC-MS/MS analysis of lower-Mw gel fragments revealed an abundance of TRIM5-derived peptides only in reactions containing proteasomes (Figure 5K, bands c and d). Incubation of Ub(GA)RB with proteasomes in the absence of N-K63-Ub did not drive equivalent TRIM5 degradation (Figure S5F). These experiments suggest that N-K63-Ub also facilitates TRIM5 proteasomal degradation.

Assembly-dependent TRIM5 NF-κB activation suggests the system has evolved to ensure innate immune stimulation only occurs following recognition of incoming virus. However, TRIM5 is capable of spontaneous self-assembly and undergoes turnover in the absence of virus, presumably without inflammatory signaling. We therefore investigated the consequences of priming ubiquitination prior to TRIM5 assembly. Surprisingly, stably expressed Ub(GA)TRIM5 was devoid of restriction activity

(K) Left: Coomassie-stained gel of reactions between Ub(GA)RB with and without prior Ub conjugation by 2N/V2, and proteasomes. Bands excised for LC-MS/MS analysis labeled a–d. X indicates the degradation product. Right: unique Ub(GA)RB peptides detected. Bottom: regions (i–iii) of Ub(GA)RB from which specific peptides were detected. Representative of three experiments.

(L) Model, TRIM5 stimulates NF-κB and proteasome degradation via an N-K63-Ub tag.

All data are representative of at least two replicates. Error bars represent SD. See also Figure S5.

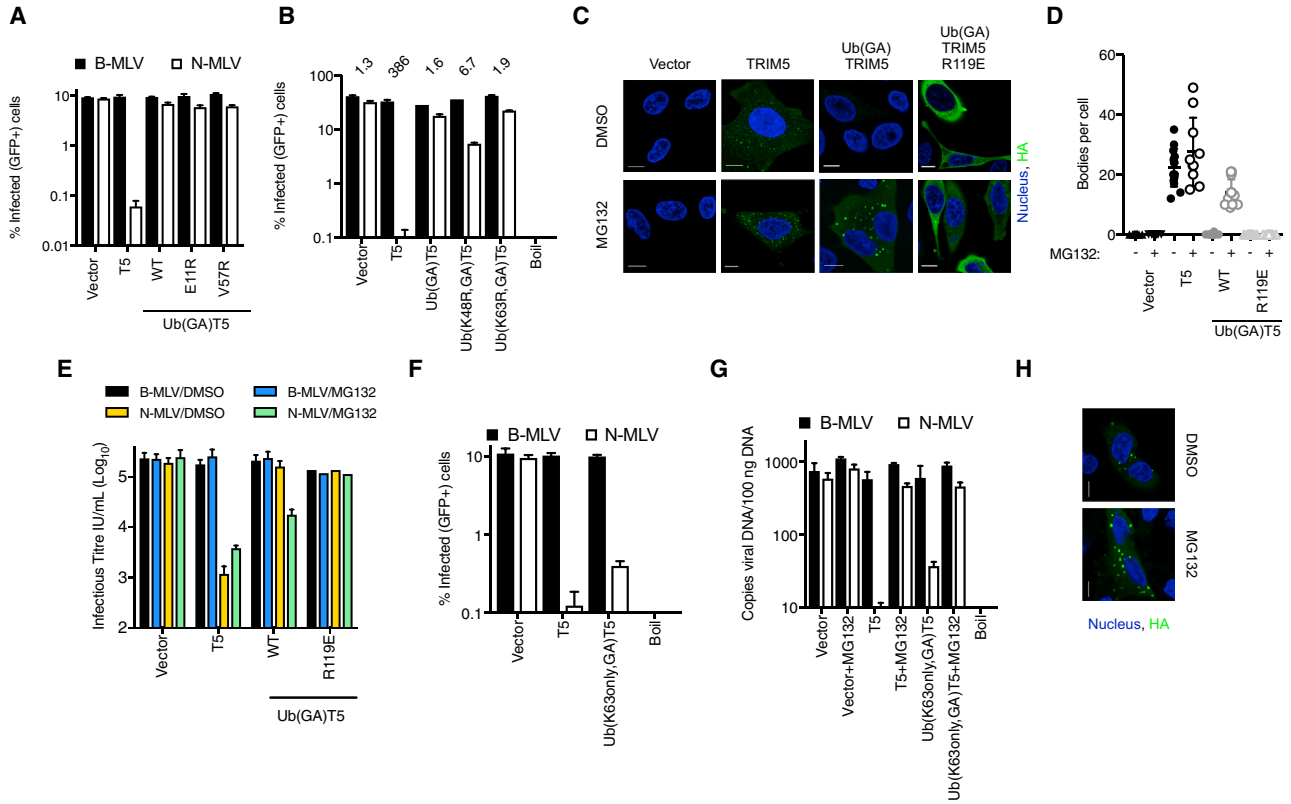

Figure 6. N-Terminal Ubiquitination before TRIM5 Assembly Causes Premature Proteasome Recruitment

(A and B) CrFK cells expressing WT or Ub(GA)TRIM5 RING mutants (A) or Ub mutants (B), infected with N-MLV- or B-MLV-GFP; percentage infection quantified by flow cytometry.

(C) Representative confocal fluorescence images of CrFK cells expressing constructs indicated, treated with DMSO or 10 μM MG132, detecting HA tag or DNA.

(D) Number of visible CBs per cell, from (C).

(E) CrFK cells from (C) infected with N-MLV- or B-MLV-GFP, percentage infection quantified by flow cytometry.

(F and G) CrFK cells expressing constructs indicated, infected with N-MLV- or B-MLV-GFP, percentage infection quantified by flow cytometry (F) or viral DNA copies quantified by TaqMan GFP qPCR (G). In (G), cells were also treated with DMSO or 10 μM MG132. Boiled virus served as a control for plasmid contamination.

(H) Representative confocal fluorescence images of CrFK cells expressing Ub(K63only,GA)TRIM5-HA, treated with DMSO or 10 μM MG132, detecting HA tag or DNA.

All data are representative of at least two replicates. Error bars represent SD.

(Figure 6A), despite no changes having been made in TRIM5 itself. The Ub fusion degradation (UFD) machinery constitutes several E3s that recognize N-terminal Ub and direct it to the proteasome (Johnson et al., 1995; Zhao and Ulrich, 2010). Given K11, K29, and K48 of Ub(GA)TRIM5 were also ubiquitinated (Figure 5D), we reasoned that lack of restriction by Ub(GA)TRIM5 could be due to premature proteasome recruitment via the UFD. Indeed, ablating TRIM5 autoubiquitination and proteasome recruitment with mutants E11R or V57R (Figure 2) did not rescue the antiviral activity of Ub(GA)TRIM5 (Figure 6A). We observed a modest rescue in restriction by mutating K48, but not K63, to arginine in Ub(GA)TRIM5 (Figure 6B), supporting UFD involvement. Strikingly, however, while WT formed numerous CBs per cell, stably expressed Ub(GA)TRIM5 formed no visible CBs (Figures 6C and 6D), consistent with pre-assembly degradation. However, Ub(GA)TRIM5 could form CBs under MG132 treatment (Figures 6C and 6D) and, critically, MG132 also restored viral restriction activity (Figure 6E). Like WT TRIM5 (Figure 1), restriction of infection was entirely dependent on higher-order assembly, as shown by Ub(GA)TRIM5 R119E neither forming CBs nor restricting infection in the presence of MG132 (Figures 6C–6E). Next, we mutated all lysines, except K63, in the N-monoUb of Ub(GA)TRIM5. We did this because K63 is a UFD target, and the TRIM5 RING, using 2N/V2, exclusively targets N-monoUb K63 (Figure 5E). Remarkably, this manipulation also restored viral restriction to Ub(GA)TRIM5 (Figure 6F). Thus protected from the UFD pathway, Ub(K63only,GA)TRIM5 restricted viral DNA synthesis in a proteasome inhibitor (MG132)-sensitive way (Figure 6G) and formed WT-like CBs that enlarged on MG132 treatment (Figure 6H), indicative of K63-Ub-dependent proteasome recruitment. We conclude that the UFD pathway, via non-K63 ubiquitination, precludes CB formation in the absence of a virus. On recruitment of TRIM5 to viral capsid, formation of N-K63 chains, catalyzed by TRIM5 itself, overwhelms local UFD activity to drive innate immune signal activation.

We next asked what property of TRIM5 assembly favored inflammatory N-K63-Ub synthesis, hypothesizing that the 3-fold

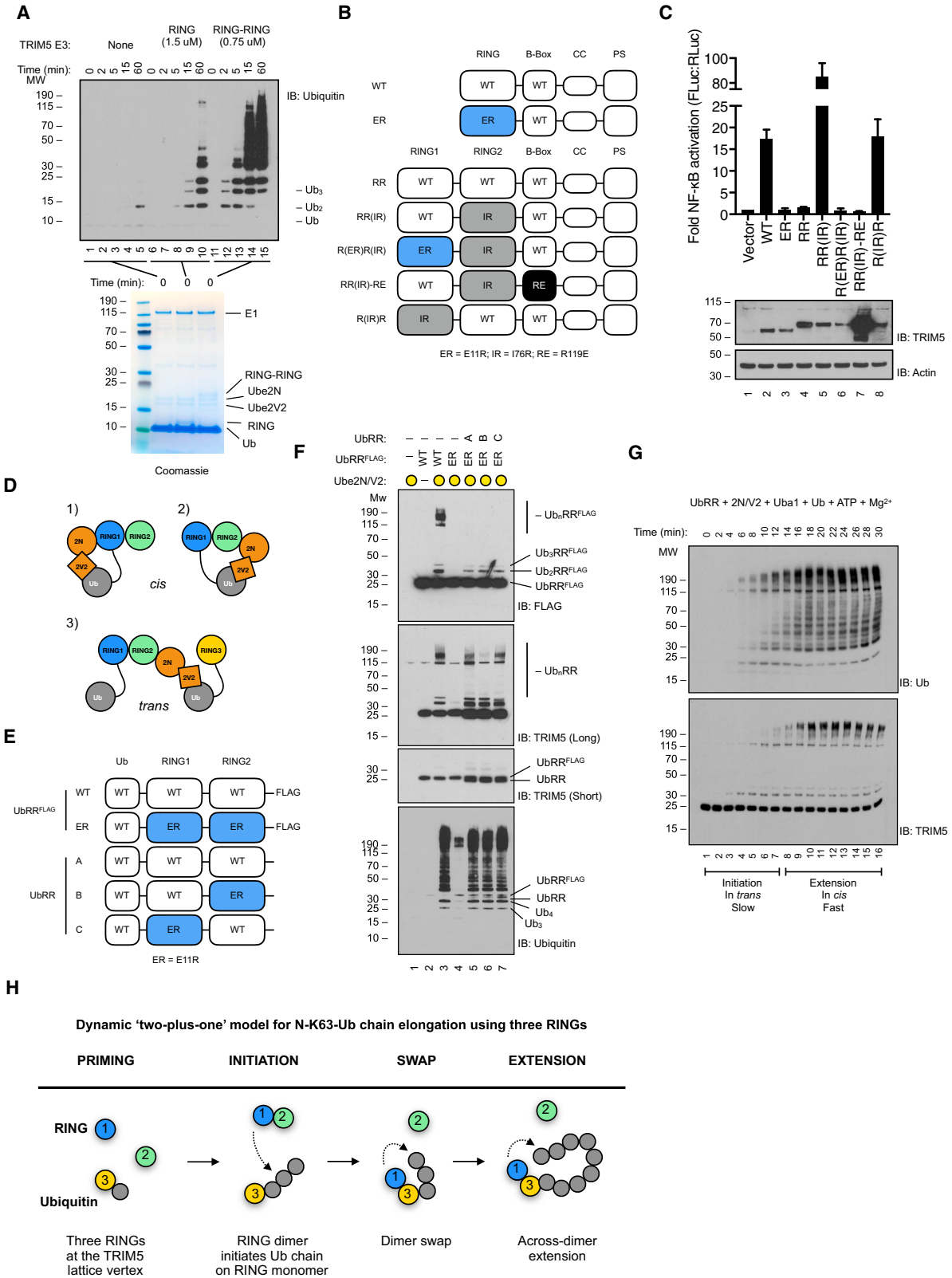

Figure 7. TRIM5 N-Terminal K63-Ub Extension Requires Three RING Domains

(A) Top: immunoblot of *in vitro* reactions between TRIM5 RING or fused RING-RING, and 2N/V2, detecting Ub. Bottom: Coomassie gel showing loading of E3s.
(B) Schematic of full-length tandem RING TRIM5 constructs generated.

(legend continued on next page)

RING arrangement could be significant. Yudina et al. (2015) suggested that RING dimerization allows unanchored Ub chains to be synthesized at the 3-fold vertex to enable antiviral activity. To bias TRIM5 ligase activity toward free Ub chain synthesis, we constructed and purified a recombinant tandem RING protein, connected by a two-residue linker, including sufficient RING residues to form the "four-helix bundle" that allows RING dimerization (Koliopoulos et al., 2016; Sanchez et al., 2016; Yudina et al., 2015). Despite normalizing for RING domain concentration, the constitutive RING dimer was significantly more effective at generating free Ub chains than a single RING (Figure 7A). We then substituted the tandem RING for the single RING in full-length TRIM5 (Figure 7B). However, RING-RING-TRIM5 was inactive for NF-κB activation in cells (Figure 7C). Strikingly, introducing the I76R RING dimer interface mutation into either of the fused RING domains restored activity, demonstrating that constitutive dimerization negatively affected activity (Figures 7B and 7C). Restored signaling was both E2 and assembly dependent, as shown by the inhibitory effects of E11R or R119E mutations, respectively (Figures 7B and 7C). Thus, free chain synthesis *in vitro* is not predictive of cellular signal activation.

Alternatively, we envisaged that a RING monomer could ubiquitinate itself (Figure 7D model 1), or a RING monomer could ubiquitinate its partner in the dimer (Figure 7D model 2). However, existing RING:E2 structures suggest 2N/V2 cannot reach an N-monoUb attached to the same RING dimer to which the E2 is bound (Figure S6B), disfavoring these *cis* models. A third scenario is that a RING dimer conjugates Ub to the third monomeric RING in *trans* (Li et al., 2016; Wagner et al., 2016; Yudina et al., 2015) (Figure 7D model 3). To test this, we designed a "ubiquitination rescue" experiment, whereby we incubated a catalytically dead TRIM5 E3 with a catalytically active TRIM5 E3 to monitor labeling of the dead substrate in *trans*. To the tandem RING protein, we genetically installed non-hydrolyzable Ub at its N terminus, and a FLAG tag at the C terminus ($UbRR^{FLAG}$) (Figure 7E). Incubation of $UbRR^{FLAG}$ (WT) with 2N/V2 led to TRIM5-anchored Ub chains (Figure 7F). As expected, chain extension was Ub K63 and Ube2V2 dependent (Figure S6C). To inactivate this E3, we introduced E11R substitutions into both RING domains (ER). This protein remained completely unmodified in the presence of 2N/V2 (Figure 7F). However, when incubated with equimolar amounts of a non-FLAG-tagged UbRR dimer (hence invisible to FLAG-specific antibodies) ER became modified, as detected by western blot (Figure 7F). This demonstrated that TRIM5 ubiquitination could occur in *trans* between a RING dimer and an adjacent N-monoUb-RING.

However, *trans* polyUb extension was inefficient, extending by 2–3 Ub molecules only (Figure 7F). Surprisingly, detection of total TRIM5 revealed that FLAG-less UbRR protein had fully extended its N-monoUb into a high-Mw chain (Figure 7F, lane 5). This indicated that intra-dimer *cis* Ub chain extension had also occurred. We repeated ubiquitination rescue experiments using unlabeled UbRR proteins bearing an E11R mutation in one or other RING domain (Figures 7E and 7F), revealing that mutation of RING2, opposite monoubiquitinated RING1, completely abrogated *cis* Ub chain extension. By contrast, synthesis of unanchored Ub chains did not require cooperation between multiple RINGs (Figure 7F). Accepting the structural limitations presented by available models (Figure S6B), these data suggest that a *trans* reaction between a RING dimer and a monomeric N-monoUb-RING can initiate an N-terminal Ub chain (2–3 Ub molecules). Ube2V2 can then coordinate the outermost Ub given the additional chain length provided (Figure S6B), and intra-dimer *cis* extension preferentially occurs. Supporting this, N-K63-Ub synthesis displayed two-step kinetics in a time-course experiment. Although free Ub chain synthesis by UbRR occurred in a stepwise fashion, whereby all intermediate chain lengths were detected, only species representing an initiated N-K63-Ub, or a fully extended N-K63-Ub, were identified. Initiated Ub chains appeared within 4 min, and fully extended Ub chains formed after another 4 min (Figure 7G), supporting a model of inefficient chain initiation in *trans* followed by efficient chain extension in *cis*.

DISCUSSION

Here we propose a mechanism by which TRIM5 uses capsid binding and autoubiquitination to translate virus recognition into inflammatory signaling. TRIM5 forms a lattice of hexagonal geometry that localizes RING domains into dynamic "two-plus-one" constellations. Our data suggest that, rather than the monomeric RING acting as a target-only "orphan" during ubiquitination, the unique trimeric RING arrangement is a specific catalytic requirement wherein all three modules are active and undergo partner exchange in order to extend N-K63-Ub chains on TRIM5 (Figure 7H). TRIM5 RING dimers are energetically weak (Figure S1A), supporting such a model.

We identify the N terminus as the authentic site of TRIM5 autoubiquitination in cells. Previously, we were unable to identify this site, because the TRIM5 extracted from cells under non-denaturing conditions was acetylated at its N terminus (Fletcher et al., 2015). Under non-denaturing conditions, all spatiotemporal cellular regulation is disrupted, meaning that non-physiological enzymatic reactions can take place. In the present study, we used denaturing conditions to preserve protein chemistries that are present before the cells are lysed and processed. Using these more stringent conditions, we find evidence for non-acetylated TRIM5 N termini by mass spectrometry. We employ N-monoUb-specific antiserum to confirm 2W-dependent N-monoUb on TRIM5 in cells (Figure 4) and demonstrate

(C) Top: NF-κB-Luc activation in 293T by constructs listed in (B). Bottom: immunoblot detecting TRIM5 and β-actin.
(D) Three models for Ub chain extension from N-monoUb by 2N/V2 in a three-RING arrangement.
(E) Schematic of recombinant Ub(GA)RING-RING proteins purified.
(F) Immunoblots of *in vitro* reactions between proteins listed in (E) and 2N/V2, detecting FLAG tag, TRIM5 or Ub.
(G) Immunoblot of time course of *in vitro* reaction between UbRR and 2N/V2, detecting TRIM5 or Ub.
(H) Schematic of a dynamic two-plus-one RING arrangement. A chain is initiated via addition of 2–3 Ub molecules to an N-monoUb, by 2N/V2 bound to an adjacent RING dimer. RINGs exchange partners and further elongation by 2N/V2 can proceed across the RING dimer.
All data are representative of at least two replicates. Error bars represent SD.

in vitro, and in cells, that monoubiquitination at this position initiates K63-Ub anchoring to TRIM5 (Figure 5). As our mass spectrometry was not quantitative, it is possible that subpopulations of TRIM5 exist, each bearing distinct N-terminal chemistries in a location-, time-, or stimulation-dependent fashion. Nonetheless, the distinctive site of TRIM5 autoubiquitination led us to explore a role for the UFD pathway in TRIM5 function. In cells where TRIM5 is functionally and stably expressed, Ub fusion drives non-productive TRIM5 turnover before higher-order structures accumulate. This is important as only during higher-order assembly (e.g., during virus recognition) does TRIM5 convert monoubiquitination from an innocuous degradation tag into an inflammatory and proteasome recruitment signal.

The evolution of N-terminal ubiquitination and a two-plus-one mechanism is likely a consequence of TRIM5's functional and regulatory requirements. TRIM5 must respond rapidly to incoming virus and is only effective within a very limited time window, before the viral capsid has accessed the nuclear pore. Consequently, TRIM5 is poised to assemble around the viral capsid and has evolved an intrinsic tendency toward self-association. While advantageous for viral restriction, which only requires caging of the virus and not ubiquitination (Figure 1), this risks triggering innate immune activation in the absence of infection (Figure 3). We propose that, by marking itself with an N-monoUb tag early during assembly, TRIM5 gains access to the UFD machinery, constitutive turnover, and negative regulation in the absence of infection (Figure S6D). Importantly, an N-monoUb tag ensures that TRIM5 levels do not breach a signaling threshold, either during constitutive expression or during interferon stimulation, yet are sufficient to intercept an incoming virus. Another advantage of N-terminal ubiquitination could be that, being largely protein sequence independent, it allows unconstrained TRIM5 evolution in pursuit of highly variable retroviral capsids.

We demonstrate that TRIM5 autoubiquitination is the signal for its own degradation by proteasomes. Such a mechanism explains why RING mutants that impair TRIM5 ubiquitination also abolish TRIM5 turnover and restriction of vDNA synthesis. This result also explains the observation that ectopic expression of K63R Ub in cells specifically impaired restriction of vDNA synthesis but not restriction of infection (Fletcher et al., 2015). How N-K63-Ub leads to proteasome recruitment and immune signaling in cells remains to be seen. Notably, proteins with disordered N termini accumulate in testes of 2W knockout mice (Wang et al., 2016), supporting a pivotal role for N-monoUb in proteasome targeting. One possibility is that secondary Ub linkages promote proteasome recruitment. Because TRIM5 and the UFD machinery both branch Ub chains from N-monoUb (Figures 4 and 5) (Johnson et al., 1995), it is possible that the UFD also recruits proteasomes to the assembled N-K63-Ub-TRIM5-virus complex. Alternatively, Ub chain branching from the N-K63-Ub scaffold could facilitate proteasome recruitment (Ohtake et al., 2018), because K63R Ub expression also abolished all TRIM5 polyUb labeling (Fletcher et al., 2015). Consistent with this hypothesis, branched K48-K63 Ub chains exhibit the combined phenotype of each individual linkage (Nakasone et al., 2013) and underlie NF-κB activation by the TRIM-related RING Ub ligase TRAF6 (Ohtake et al., 2016). Synchronization of proteasome recruitment with innate immune signaling is suggested by the observations that incoming virus enhances both TRIM5 turnover (Rold and Aiken, 2008) and immune signaling (Figure 3) (Pertel et al., 2011).

Higher-order assembly is a central theme in innate immunity, whereby transient signal activation occurs via colocalization of weakly interacting intermediates, exemplified by inflammasomes and the CARMA1-BCL10-MALT1-TRAF6 signalosome (David et al., 2018; Hauenstein et al., 2015). During infection, TRIM5 uses higher-order assembly to promote capsid binding through avidity. Our identification of CBs as signaling hubs suggests that the TRIM5 lattice is in fact a pathogen-templated signaling platform. A remarkable regulatory feature of this system is that it is intrinsically self-limiting, because the same Ub signal that stimulates immune signaling drives CB turnover. A correlation between CB assembly and immunostimulation was also observed in specific murine TRIM5 homologues (Lascano et al., 2015), suggesting that this might be a unifying feature of TRIM5-like proteins and perhaps of other immune TRIMs too.

STAR★METHODS

Detailed methods are provided in the online version of this paper and include the following:

- KEY RESOURCES TABLE
- CONTACT FOR REAGENT AND RESOURCE SHARING
- EXPERIMENTAL MODEL AND SUBJECT DETAILS
  - Cell Lines
  - Animal Husbandry
  - Bacteria
- METHOD DETAILS
  - Virus Restriction Assays
  - Viral Vectors, Mutant cDNAs
  - Cloning
  - Protein Depletion
  - Cycloheximide Chase and Immunoblotting
  - Innate Immune Stimulation Experiments
  - Recombinant Protein Purification
  - Cellular Proteasome Purification
  - Immunoprecipitations and His-Pulldowns
  - In Vitro Ub Assays
  - Confocal Microscopy
  - Mouse Immunizations
  - ELISA
  - SEC-MALLS
- QUANTIFICATION AND STATISTICAL ANALYSIS

SUPPLEMENTAL INFORMATION

Supplemental Information includes six figures and two tables can be found with this article online at https://doi.org/10.1016/j.chom.2018.10.007.

ACKNOWLEDGMENTS

We thank Claire Dickson for providing recombinant TRIM5 RING, Ube2W, and Ube2N; Donna Mallery for providing recombinant Ube2V2; Chris Johnson for assistance with SEC-MALLS experiments; and Jonathan Pruneda for critical reading of the manuscript, experimental advice, and recombinant K63R Ub. L.C.J. received funding from the Medical Research Council (UK; U105181010) and through a Wellcome Trust Investigator Award; G.J.T. received funding through a Wellcome Trust Senior Biomedical Research

Fellowship and the European Research Council grant agreement number 339223; and A.J.F., M.V., S.M., and J.M.S. were all supported by the Medical Research Council.

AUTHOR CONTRIBUTIONS

A.J.F., G.J.T., and L.C.J. conceived the project. A.J.F. designed and performed the experiments. M.V. planned mouse immunizations, collected immune sera, and performed ELISA. J.Z. assisted with human cell reconstitution assays. S.M. and J.M.S. prepared samples and performed mass spectrometry experiments. A.J.F., G.J.T., and L.C.J. wrote the manuscript.

DECLARATION OF INTERESTS

The authors declare no competing interests.

Received: May 31, 2018
Revised: August 31, 2018
Accepted: October 16, 2018
Published: November 29, 2018

REFERENCES

Branigan, E., Plechanovova, A., Jaffray, E.G., Naismith, J.H., and Hay, R.T. (2015). Structural basis for the RING-catalyzed synthesis of K63-linked ubiquitin chains. Nat. Struct. Mol. Biol. *22*, 597–602.

Campbell, E.M., Perez, O., Anderson, J.L., and Hope, T.J. (2008). Visualization of a proteasome-independent intermediate during restriction of HIV-1 by rhesus TRIM5alpha. J. Cell Biol. *180*, 549–561.

Campbell, E.M., Weingart, J., Sette, P., Opp, S., Sastri, J., O'Connor, S.K., Talley, S., Diaz-Griffero, F., Hirsch, V., and Bouamr, F. (2015). TRIM5alpha-mediated ubiquitin chain conjugation is required for inhibition of HIV-1 reverse transcription and capsid destabilization. J. Virol. *90*, 1849–1857.

David, L., Li, Y., Ma, J., Garner, E., Zhang, X., and Wu, H. (2018). Assembly mechanism of the CARMA1-BCL10-MALT1-TRAF6 signalosome. Proc. Natl. Acad. Sci. U S A *115*, 1499–1504.

Diaz-Griffero, F., Li, X., Javanbakht, H., Song, B., Welikala, S., Stremlau, M., and Sodroski, J. (2006). Rapid turnover and polyubiquitylation of the retroviral restriction factor TRIM5. Virology *349*, 300–315.

Diaz-Griffero, F., Kar, A., Perron, M., Xiang, S.H., Javanbakht, H., Li, X., and Sodroski, J. (2007). Modulation of retroviral restriction and proteasome inhibitor-resistant turnover by changes in the TRIM5alpha B-box 2 domain. J. Virol. *81*, 10362–10378.

Fletcher, A.J., Christensen, D.E., Nelson, C., Tan, C.P., Schaller, T., Lehner, P.J., Sundquist, W.I., and Towers, G.J. (2015). TRIM5alpha requires Ube2W to anchor Lys63-linked ubiquitin chains and restrict reverse transcription. EMBO J. *34*, 2078–2095.

Ganser-Pornillos, B.K., Chandrasekaran, V., Pornillos, O., Sodroski, J.G., Sundquist, W.I., and Yeager, M. (2011). Hexagonal assembly of a restricting TRIM5alpha protein. Proc. Natl. Acad. Sci. U S A *108*, 534–539.

Goldstone, D.C., Walker, P.A., Calder, L.J., Coombs, P.J., Kirkpatrick, J., Ball, N.J., Hilditch, L., Yap, M.W., Rosenthal, P.B., Stoye, J.P., et al. (2014). Structural studies of postentry restriction factors reveal antiparallel dimers that enable avid binding to the HIV-1 capsid lattice. Proc. Natl. Acad. Sci. U S A *111*, 9609–9614.

Han, K., Lou, D.I., and Sawyer, S.L. (2011). Identification of a genomic reservoir for new TRIM genes in primate genomes. PLoS Genet. *7*, e1002388.

Hauenstein, A.V., Zhang, L., and Wu, H. (2015). The hierarchical structural architecture of inflammasomes, supramolecular inflammatory machines. Curr. Opin. Struct. Biol. *31*, 75–83.

Johnson, E.S., Ma, P.C., Ota, I.M., and Varshavsky, A. (1995). A proteolytic pathway that recognizes ubiquitin as a degradation signal. J. Biol. Chem. *270*, 17442–17456.

Johnston, J.A., Ward, C.L., and Kopito, R.R. (1998). Aggresomes: a cellular response to misfolded proteins. J. Cell Biol. *143*, 1883–1898.

Koliopoulos, M.G., Esposito, D., Christodoulou, E., Taylor, I.A., and Rittinger, K. (2016). Functional role of TRIM E3 ligase oligomerization and regulation of catalytic activity. EMBO J. *35*, 1204–1218.

Kutluay, S.B., Perez-Caballero, D., and Bieniasz, P.D. (2013). Fates of retroviral core components during unrestricted and TRIM5-restricted infection. PLoS Pathog. *9*, e1003214.

Lascano, J., Uchil, P.D., Mothes, W., and Luban, J. (2015). TRIM5 retroviral restriction activity correlates with the ability to induce innate immune signaling. J. Virol. *90*, 308–316.

Li, X., and Sodroski, J. (2008). The TRIM5alpha B-box 2 domain promotes cooperative binding to the retroviral capsid by mediating higher-order self-association. J. Virol. *82*, 11495–11502.

Li, Y.L., Chandrasekaran, V., Carter, S.D., Woodward, C.L., Christensen, D.E., Dryden, K.A., Pornillos, O., Yeager, M., Ganser-Pornillos, B.K., Jensen, G.J., et al. (2016). Primate TRIM5 proteins form hexagonal nets on HIV-1 capsids. eLife *5*, https://doi.org/10.7554/eLife.16269.

Nakasone, M.A., Livnat-Levanon, N., Glickman, M.H., Cohen, R.E., and Fushman, D. (2013). Mixed-linkage ubiquitin chains send mixed messages. Structure *21*, 727–740.

Ohtake, F., Saeki, Y., Ishido, S., Kanno, J., and Tanaka, K. (2016). The K48-K63 branched ubiquitin chain regulates NF-kappaB signaling. Mol. Cell *64*, 251–266.

Ohtake, F., Tsuchiya, H., Saeki, Y., and Tanaka, K. (2018). K63 ubiquitylation triggers proteasomal degradation by seeding branched ubiquitin chains. Proc. Natl. Acad. Sci. U S A *115*, E1401–E1408.

Pertel, T., Hausmann, S., Morger, D., Zuger, S., Guerra, J., Lascano, J., Reinhard, C., Santoni, F.A., Uchil, P.D., Chatel, L., et al. (2011). TRIM5 is an innate immune sensor for the retrovirus capsid lattice. Nature *472*, 361–365.

Roa, A., Hayashi, F., Yang, Y., Lienlaf, M., Zhou, J., Shi, J., Watanabe, S., Kigawa, T., Yokoyama, S., Aiken, C., et al. (2012). RING domain mutations uncouple TRIM5alpha restriction of HIV-1 from inhibition of reverse transcription and acceleration of uncoating. J. Virol. *86*, 1717–1727.

Rold, C.J., and Aiken, C. (2008). Proteasomal degradation of TRIM5alpha during retrovirus restriction. PLoS Pathog. *4*, e1000074.

Sanchez, J.G., Chiang, J.J., Sparrer, K.M.J., Alam, S.L., Chi, M., Roganowicz, M.D., Sankaran, B., Gack, M.U., and Pornillos, O. (2016). Mechanism of TRIM25 catalytic activation in the antiviral RIG-I pathway. Cell Rep. *16*, 1315–1325.

Sanchez, J.G., Okreglicka, K., Chandrasekaran, V., Welker, J.M., Sundquist, W.I., and Pornillos, O. (2014). The tripartite motif coiled-coil is an elongated antiparallel hairpin dimer. Proc. Natl. Acad. Sci. U S A *111*, 2494–2499.

Stremlau, M., Owens, C.M., Perron, M.J., Kiessling, M., Autissier, P., and Sodroski, J. (2004). The cytoplasmic body component TRIM5alpha restricts HIV-1 infection in Old World monkeys. Nature *427*, 848–853.

Tatham, M.H., Plechanovova, A., Jaffray, E.G., Salmen, H., and Hay, R.T. (2013). Ube2W conjugates ubiquitin to alpha-amino groups of protein N-termini. Biochem. J. *453*, 137–145.

Vittal, V., Shi, L., Wenzel, D.M., Scaglione, K.M., Duncan, E.D., Basrur, V., Elenitoba-Johnson, K.S., Baker, D., Paulson, H.L., Brzovic, P.S., et al. (2015). Intrinsic disorder drives N-terminal ubiquitination by Ube2w. Nat. Chem. Biol. *11*, 83–89.

Wagner, J.M., Roganowicz, M.D., Skorupka, K., Alam, S.L., Christensen, D., Doss, G., Wan, Y., Frank, G.A., Ganser-Pornillos, B.K., Sundquist, W.I., et al. (2016). Mechanism of B-box 2 domain-mediated higher-order assembly of the retroviral restriction factor TRIM5alpha. eLife *5*, https://doi.org/10.7554/eLife.16309.

Wang, B., Merillat, S.A., Vincent, M., Huber, A.K., Basrur, V., Mangelberger, D., Zeng, L., Elenitoba-Johnson, K., Miller, R.A., Irani, D.N., et al. (2016). Loss of the ubiquitin-conjugating enzyme UBE2W results in susceptibility to early postnatal lethality and defects in skin, immune, and male reproductive systems. J. Biol. Chem. *291*, 3030–3042.

Wang, X., Chen, C.F., Baker, P.R., Chen, P.L., Kaiser, P., and Huang, L. (2007). Mass spectrometric characterization of the affinity-purified human 26S proteasome complex. Biochemistry *46*, 3553–3565.

Wu, X., Anderson, J.L., Campbell, E.M., Joseph, A.M., and Hope, T.J. (2006). Proteasome inhibitors uncouple rhesus TRIM5alpha restriction of HIV-1 reverse transcription and infection. Proc. Natl. Acad. Sci. U S A *103*, 7465–7470.

Yudina, Z., Roa, A., Johnson, R., Biris, N., de Souza Aranha Vieira, D.A., Tsiperson, V., Reszka, N., Taylor, A.B., Hart, P.J., Demeler, B., et al. (2015). RING dimerization links higher-order assembly of TRIM5alpha to synthesis of K63-linked polyubiquitin. Cell Rep. *12*, 788–797.

Zhao, S., and Ulrich, H.D. (2010). Distinct consequences of posttranslational modification by linear versus K63-linked polyubiquitin chains. Proc. Natl. Acad. Sci. U S A *107*, 7704–7709.

STAR★METHODS

KEY RESOURCES TABLE

REAGENT or RESOURCE	SOURCE	IDENTIFIER
Antibodies		
Mouse monoclonal anti-TRIM5 (5D5-1-1)	Aids Reagents	Cat#12272
Mouse monoclonal anti-β-actin-HRP (C4)	Santa Cruz	Cat#sc-47778 HRP, RRID: AB_2714189
Rat monoclonal anti-HA-HRP (3F10)	Sigma-Aldrich	Cat#12013819001, RRID: AB_390917
Rabbit polyclonal anti-HA	Abcam	Cat#ab9110, RRID: AB_307019
Mouse monoclonal anti-HA (16B12)	BioLegend	Cat#901501, RRID: AB_2565006
Mouse monoclonal anti-Ub-HRP (P4D1)	Santa Cruz	Cat#sc-8017, RRID: AB_628423
Mouse monoclonal anti-IκBα (L35A5)	Cell Signaling Technology	Cat#4814, RRID: AB_390781
Mouse monoclonal anti-phospho-IκBα (Ser32/36)	Cell Signaling Technology	Cat#9246, RRID: AB_2267145
Mouse monoclonal anti-NF-κB p65 (F-6)	Santa Cruz	Cat#sc-8008, RRID: AB_628017
Mouse polyclonal anti-N-monoUb	This paper	N/A
Mouse polyclonal anti-TRIM21 RING-B-Box2	This paper	N/A
Rabbit polyclonal anti-GFP	Abcam	Cat#ab6556, RRID: AB_305564
Rabbit polyclonal anti-Ube2N	BioRad	Cat#AHP974, RRID: AB_567248
Donkey anti-Mouse IgG Alexa Fluor 488	Life Technologies	Cat#A21202, RRID: AB_141607
Donkey anti-Rabbit IgG Alexa Fluor 568	Life Technologies	Cat#A10042, RRID: AB_2534017
Rabbit monoclonal anti-PSMD14 (EPR4258)	Abcam	Cat#ab109130, RRID: AB_10861705
Mouse monoclonal anti-20Sα 1+2+3+5+6+7 (MCP231)	Abcam	Cat#ab22674, RRID: AB_2171376
Rabbit monoclonal anti-UCH37 (EP4897)	Abcam	Cat#ab133508
Rabbit monoclonal anti-USP14 (EPR15943)	Abcam	Cat#ab192618
Rabbit monoclonal anti-ADRM1 (EPR11450(B))	Abcam	Cat#157218
Goat anti-Mouse IgG (Fc specific)-Peroxidase	Sigma-Aldrich	Cat#A0168, RRID: AB_257867
Goat anti-Rabbit IgG, HRP-linked	Cell Signaling Technology	Cat#7074, RRID: AB_2099233
Normal mouse polyclonal IgG control	Merck Millipore	Cat#12-371, RRID: AB_145840
Bacterial and Virus Strains		
E. coli DH10B chemically competent	Thermo Fisher	Cat#18297010
E. coli C41 chemically competent	John Walker	N/A
Chemicals, Peptides, and Recombinant Proteins		
Polybrene	Santa-Cruz	Cat#sc-134220
MG132	Calbiochem	Cat#474790
Cycloheximide	Calbiochem	Cat#508739
Human TNFα	PeproTech	Cat#300-01A
Protein G Sepharose	Generon	Cat#PC-G5
Glutathione Sepharose 4B	GE Healthcare	Cat#17-0756-01
RING-B-Box2 (residues 1-132)	This paper	N/A
RING(E11R)-B-Box2	This paper	N/A
RING(L19R)-B-Box2	This paper	N/A
RING(V57R)-B-Box2	This paper	N/A
RING(N70A)-B-Box2	This paper	N/A
RING(V73A)-B-Box2	This paper	N/A
RING(I76R)-B-Box2	This paper	N/A
RING (residues 1- 87)	This paper	N/A
RING-GS-RING	This paper	N/A
UbRING-B-Box2	This paper	N/A
Ub(G75/76A)RING-B-Box2	This paper	N/A

(*Continued on next page*)

Continued

REAGENT or RESOURCE	SOURCE	IDENTIFIER
Ub(G75/76A)RING(E11R)-B-Box2	This paper	N/A
Ub(K63R,G75/76A)RING-B-Box2	This paper	N/A
Ub(I44A,A46E,G47E,G75/76A)RING-B-Box2	This paper	N/A
Ub(G75/76A)RING-GS-RING-Flag	This paper	N/A
Ub(G75/76A)RING(E11R)-GS-RING(E11R)-Flag	This paper	N/A
Ub(G75/76A)RING-GS-RING	This paper	N/A
Ub(G75/76A)RING-GS-RING(E11R)	This paper	N/A
Ub(G75/76A)RING(E11R)-GS-RING	This paper	N/A
RING-B-Box2 (residues 1-132)	This paper	N/A
Ubel	This paper	N/A
Ube2W	(Fletcher et al., 2015)	N/A
Ube2N	(Fletcher et al., 2015)	N/A
Ube2N(K92R)	This paper	N/A
Ube2V2	This paper	N/A
Ubiquitin	This paper	N/A
Human 20S Proteasome	BostonBiochem	Cat#E-360; Lot#21118515D
Human 19S Proteasome	BostonBiochem	Cat#E-366; Lot#26730315A
Critical Commercial Assays		
Dual Luciferase Reporter Assay System	Promega	Cat#E1910
RNeasy mini kit	Qiagen	Cat#74104
Gibson Assembly Master Mix	New England BioLabs	Cat#E2611
Experimental Models: Cell Lines		
Human: Embryonic kidney 293T cells	ATCC	Cat#CRL-3216
Human: Rhabdomyosarcoma TE671 cells	ATCC	Cat#HTB-139
Human: Peripheral blood monocytic THP-1 cells	ATCC	Cat#TIB-202
Feline: Kidney epithelial CrFK cells	ATCC	Cat#CCL-94
Oligonucleotides		
shRNA targeting sequence: TRIM5: CAGCCTTTCTATATCATCG	(Stremlau et al., 2004)	N/A
shRNA targeting sequence: Ube2W: GCATGATAGGGCCTATGAA	(Fletcher et al., 2015)	N/A
shRNA scrambled sequence: GTTATAGGCTCGCAAAAGG	(Fletcher et al., 2015)	N/A
sgRNA targeting TRIM5: CCTCCTCCTTTACATTAACC	This paper	sgRNA 'D'
TaqMan GFP 5'-3' primer: CAACAGCCACAACGTCTATATCAT	(Fletcher et al., 2015)	N/A
TaqMan GFP 3'-5' primer: ATGTTGTGGCGGATCTTGAAG	(Fletcher et al., 2015)	N/A
TaqMan Probe: 5'[6FAM]CCGACAAGCAGAAGAACGGCATC AA[TAM]3'	(Fletcher et al., 2015)	N/A
Recombinant DNA		
pCIG3-N	This group	N/A
pCIG3-B	This group	N/A
pCMV-Neo-CMV-GFP (CNCG)	Yasu Takeuchi	N/A
CSGW (cPPT-SFFV-GFP-WPRE)	Adrian Thrasher	N/A
CMVintron (CMVi) (Mo-MLV Gag-Pol)	Francoise Loic Cosset	N/A
p8.91Ex (HIV-1 Gag-Pol)	Yasu Ikeda	N/A
pMD2.G (VSV-G envelope)	GenScript	N/A
CMV-Ampho	This group	N/A
pONY3.1 (EIAV Gag-Pol)	Kyriacos Mitrophanous	N/A
pONY8.0	Kyriacos Mitrophanous	N/A
SIREN-RetroQ	Clontech	N/A
HIV-SIREN	This group	N/A
pcDNA3.1(+)	Life Technologies	N/A

(*Continued on next page*)

Continued

REAGENT or RESOURCE	SOURCE	IDENTIFIER
EXNΔHA	EXN, Paul Bieniasz	N/A
pIKK2Flag	Felix Randow	N/A
pGL4.32[luc2P/NF-kB-RE/Hygro]	Promega	Cat#9PIE849
pRL-TK	Promega	Cat#E2241
pLentiCRISPRv2	Brett Stringer	Cat#98290
pQCXIP-Rpn11-HTBH	Lan Huang	N/A
TRIM and GFP Expression Constructs for Mammalian Cells, see Table S1	This paper	N/A
TRIM Expression Constructs for Bacterial Cells, see Table S2	This paper	N/A
Software and Algorithms		
DNADynamo v1.411	Blue Tractor Software	N/A
Prism 7	GraphPad Software	N/A
FlowJo	FlowJo, LLC	N/A
Scaffold4 (LC-MS/MS)	Proteome Software	N/A
ASTRA (SEC-MALLS)	Wyatt Technology Corp	N/A

CONTACT FOR REAGENT AND RESOURCE SHARING

Further information and requests for resources and reagents should be directed to and will be fulfilled by the Lead Contact, Leo James (lcj@mrc-lmb.cam.ac.uk).

EXPERIMENTAL MODEL AND SUBJECT DETAILS

Cell Lines

Cell lines were maintained at 37°C in 5 % CO_2 humidified incubators. Culture medium was DMEM (TE671 (Human, Female), CrFK (Cat, Female) and 293T (Human Fetal)) or RPMI (THP-1 (Human, Male)), each supplemented with 9% (v/v) fetal calf serum, 100 U/mL penicillin, 100 μg/mL streptomycin. Cells were confirmed negative for mycobacteria contamination using the MycoAlert Mycoplasma Detection Kit (Lonza). The identities of these cells lines were not authenticated during the course of this study.

Animal Husbandry

C57BL/6 wild-type mice were obtained from Jackson Laboratories. Mice were bred and housed under specific pathogen-free conditions in the Animal Research facilities at the Babraham campus, Cambridge, UK. Thirteen week old-mice of both genders were used for the immunisation experiment, which was conducted in accordance with the 19.b.5 moderate severity limit protocol and Home Office Animals (Scientific Procedures) Act (1986). All animal work was licensed under the UK Animals (Scientific Procedures) Act, 1986 and approved by the Medical Research Council Animal Welfare and Ethical Review Body. Throughout the protocol, animals were weighed and observed twice daily for clinical signs of infection, which included subdued behaviour, pilo-erection, hunched posture, ataxia, and paresis. Animals that reached the end of the experiment, lost more than 20% of initial body weight, or showed clinical signs that failed to improve over a 6 hr period were killed. Serum was prepared from intracardiac blood and frozen in liquid nitrogen.

Bacteria

E. coli strain C41 was used to produce recombinant protein for biochemical characterisation experiments. C41 cells were transformed and grown at 37°C to derive single-cell colonies. Colonies were picked and grown in liquid 2xTY media overnight at 37°C, and then grown at 34°C until induction at an optical density at 600 nm of 0.8, then grown overnight at 16°C in the presence of 1 mM IPTG.

METHOD DETAILS

Virus Restriction Assays

CrFK or TE671 cells were infected with DNase-treated N-MLV- or B-MLV-GFP viral vector supernatants in the presence of 8 μg/mL polybrene. 6 hr post infection (p.i.), duplicate wells were pelleted and stored at -80°C. 48 hr p.i., duplicate wells were scored for GFP expression by flow cytometry (FACSCalibur). Total DNA was extracted from 6 hr samples using QIAamp DNA Mini Kit (Qiagen). Heat-treated viral supernatants (95°C, 5 min) served as controls for plasmid contamination. Concentration of each DNA sample was

quantified using a NanoDrop spectrophotometer ND-1000 (Thermo Fisher Scientific). TaqMan qPCR reactions contained 5 μl of eluted DNA, 300 nM forward and reverse primers against GFP, 150 nM probe, 20 μg salmon sperm DNA, and TaqMan Fast Advanced Master Mix (ThermoFisher Scientific). Standard curves generated from GFP cDNA plasmids were created for each assay. Cycle parameters for gene detection were 95°C for 20 sec, then 40 cycles of 95°C for 1 sec, 60°C for 20 sec, using a StepOnePlus thermocycler (Applied Biosystems).

Viral Vectors, Mutant cDNAs

As described (Fletcher et al., 2015), VSV-G pseudotyped viral particles were generated by three-plasmid transfection of 293T with Fugene-6 (Promega), using 1 μg Gag-Pol expression plasmid, 1 μg VSV-G expression plasmid pMD2.G (GenScript) or CMV-Ampho, and 1.5 μg genome vector encoding cDNAs or shRNAs. TRIM5 mutants were generated by site-directed mutagenesis using *Pfu*Turbo (Agilent Technologies).

Cloning

Site-directed mutagenesis was performed using *Pfu* Turbo. Synthesis of fused RING-RING constructs was carried out using Gibson cloning and Gibson Assembly Master Mix (New England BioLabs) following manufacturer's instructions.

Protein Depletion

Short-hairpin RNA (shRNA): Cells depleted of 2W or TRIM5 were prepared as described (Fletcher et al., 2015). Briefly, pSIREN-RetroQ or HIV-SIREN expressing shRNA against 2W or TRIM5, respectively, were transfected into 293T cells and MLV or HIV-1 viral vectors prepared as described. Cells were transduced at an MOI ~ 1 and shRNA-expressing cells selected with 2.5 – 10 μg/mL puromycin. 2W expression was quantified by qPCR relative to *ACTB* using TaqMan Gene Expression Assays for *2W* (Hs00217672_m1) and *ACTB* (Hs01060665_g1), by the ΔΔCt method.

CRISPR/Cas9: TE671 stably depleted of TRIM5 were generated by transduction with HIV-1-based lentivectors carrying Cas9-2A-Puromcin and single guide RNA (sgRNA) expression cassettes (pLentiCRISPRv2 Puro, a gift from Brett Stringer (Addgene plasmid # 98290). DNA oligonucleotides for generation of sgRNA were synthesised (Sigma Aldrich), annealed, and cloned into the linearized vectors. Cells were selected with Puromycin. To reconstitute these cells, TRIM5 was silently mutated at the PAM site before reintroduction by transduction with MLV vectors.

Reconstitution of TRIM5 in TRIM5 depleted cells: TRIM5 was silently mutated using forward primer (CTGGAATTTTGGTTAATG TAAAGGAGGAGG) and reverse primer (CATTAACCAAAATTCCAGAAGCCATGGTGG) to remove the PAM site for TRIM5-specific sgRNA (CCTCCTCCTTTACATTAACC). Mutant TRIM5 cDNAs were packaged in MLV viral vectors and TRIM5 depleted cells were transduced as described above.

Cycloheximide Chase and Immunoblotting

Cells expressing HA-tagged TRIM5α proteins were treated with 100 μg/mL cycloheximide for up to 6 hr, washed, lysed in 2X LDS Loading Buffer (Life Technologies) with 50 mM DTT, heated at 95°C for 5 min, then resolved by SDS-PAGE using NuPAGE 4-12 % Bis-Tris Protein Gels (Life Technologies). Proteins were transferred to nitrocellulose membranes using the iBlot Gel Transfer Device (Life Technologies). Membranes were incubated in blocking buffer (phosphate buffered saline (PBS)/0.1 % Tween-20 (PBST) containing 5 % milk), incubated in blocking buffer containing primary and secondary antibodies, 3× 5 min PBST washes after each antibody. HRP-conjugated antibodies were detected using Amersham ECL Western Blotting Detecting Reagent (GE Healthcare).

Innate Immune Stimulation Experiments

In response to virus: THP-1 cells were seeded in 24 or 96 well plates and differentiated with 100 ng/μL 12-O-Tetradecanoylphorbol-13-acetate (TPA, Sigma-Aldrich) for 24 hr, washed, incubated at 37°C for 48 hr. Then, cells were infected with N- and B-MLV pseudotyped with an MLV-amphoteric envelope glycoprotein, at MOI ~10, in the presence of 8 μg/mL polybrene (Santa Cruz). Cells were washed and frozen at -20°C at 1.5-2 hr post infection. Total RNA was extracted (Qiagen RNeasy kit) and reverse transcription performed using SuperScript II (Thermo Fisher Scientific). qPCR reactions were performed with TaqMan Gene Expression Assays (Thermo Fisher Scientific) for, *ACTB* (Hs01060665_g1), *IL6* (Hs00174131_m1), *IL1B* (Hs00174097_m1), *IFNB1 (*Hs01077958_s1), *TNFA (*Hs00174128_m1), *IFIT1* (Hs00356631_g1), *NLRP3* (Hs00366461_m1), *PTGS2* (Hs00153133_m1), *SOD2* (Hs00167309_m1), and TaqMan Fast Advanced Master Mix (Thermo Fisher Scientific). Cycle parameters for gene detection were as for detection of viral DNA above. Fold changes in mRNA were caluculated by the ΔΔCt method using *ACTB* as the uninduced control.

In response to TRIM overexpression: 293T cells were seeded in 24 well plates 24 hr before transfection. Each well was transfected with 0.3–100 ng pcDNA or EXN derived vectors containing the relevant TRIM cDNA, with 10 ng pGL4.32[*luc2P*/NF-κB-RE/Hygro] (NF-κB response element-dependent firefly luciferase, FLuc) and 5 ng pRL-TK (thymidine kinase promoter-dependent *Renilla* luciferase, RLuc). 24 hr post transfection, cells were lysed in Passive Lysis Buffer and sequential firefly and renilla luminesence measured (BMG Pherastar plate reader), according to manufacturers instructions (Promega). FLuc:RLuc ratios of each construct were normalised to those of empty vector alone.

Recombinant Protein Purification

Wild-type and N-terminal monoubiquitinated TRIM5 RING, RING-RING and RING-B-Box2 proteins, and E1, Ube2N, Ube2V2 and 2W were expressed in C41 cells as GST-TEV-fusion proteins. Cleared cell lysates were prepared by sonication in 50 mM Tris, pH 8.0, 150 mM NaCl, 2 mM DTT, 2 μM $ZnCl_2$, 1 mg/mL lysozyme, 0.1 mg/mL DNaseI with the addition of cOmplete, EDTA-free Protease Inhibitor Cocktail (Roche), followed by centrifugation at 19,000 × *g* for 1 hr at 4°C. Lysates were loaded onto equilibrated glutathione sepharose resin and washed with three column volumes of lysis buffer, then cleaved with recombinant His-TEV protease overnight at 4°C. Cleaved proteins were concentrated, His-TEV was removed on Ni^{2+}-NTA agarose, and TRIM5 or E2 proteins resolved by size-exclusion chromatography (HiLoad 26/60 Superdex 75 size exclusion column, GE Healthcare). Peak fractions were pooled, concentrated, and frozen in aliquots at -80°C. TEV cleavage leaves a GSH tripeptide at the N terminus of TRIM5 proteins. To prevent cleavage of Ub from RB by bacteria and allowing purification to homogeneity (Ub(GA)RB) (Figure S4B), we changed N-terminal Ub residues Gly75 and Gly76 to alanine.

Cellular Proteasome Purification

Cellular proteasomes were isolated using a protocol adopted from that described in Wang et al. (2007). pQCXIP-Poh1-His-TEV-Biotin-His (HTBH) was transfected into 293T cells with CMVi and pMD2.G to generate MLV viral vectors. TE671 cells were transduced with viral vectors and Poh1-HTBH was stably expressed by selection with 10 μg/mL puromycin selection. Confluent 10 cm dishes were trypsinised, washed three times with PBS, and lysed in 100 mM NaCl, 50 mM Na_2HPO_4/NaH_2PO_4, 10 % glycerol, 5 mM ATP, 1 mM DTT, 5 mM $MgCl_2$, 0.5 % NP-40, protease and phosphatase inhibitors, pH 7.5. Lysates were passed through a 25 G syringe four times then centrifuged 15,000 ×*g*, 15 min, 4°C. Insoluble material was discarded and cell lysates were incubated with equilibrated glutathione sepharose resin overnight at 4°C. Resin was washed twice with 20× bed volume of lysis buffer, 1× with 50 mM Tris pH 7.5, 10 % glycerol, and incubated for 1 hr at 22°C in the same buffer, 2× bed volume, with 30 μL recombinant His-TEV protease. The presence of 20S and 19S components was confirmed by immunoblot (see Figure S5E).

Immunoprecipitations and His-Pulldowns

Immunoprecipitations: Cells were washed twice in ice-cold PBS and collected into ice-cold lysis buffer (10 mM Tris, pH 7.4, 200 mM NaCl, 3 mM $MgCl_2$, 2 mM DTT, 0.5% Triton-X-100, cOmplete, EDTA-free Protease Inhibitor Cocktail (Roche)), 1 mL per 10 cm dish. Cells were passed 5 × through a 25 G needle, rotated at 4°C for 20 min and centrifuged at 15,000 ×*g* at 4°C for 10 min. Cell lysates were transferred to fresh tubes and 30 μL kept for 'input' fractions. Anti-N-monoUb antibodies were first pre-adsorbed on plates coated with recombinant RB protein, and added to lysates at a final concentration of 1:10,000. Lysates were rotated overnight at 4°C, then 50 μL 50% equilibrated protein G sepharose (Generon) was added per 1 mL lysate and rotated for 1–4 hr at 4°C. Sepharose was centrifuged < 1000 ×*g* for 30 sec at 4°C and washed three times. Immunoprecipitants were snap frozen on beads for LC-MS/MS analysis.

His-pulldown: As previously described (Fletcher et al., 2015). Cells were lysed in 6 M Guanidine hydrochloride pH 8, before incubation with Nickel NTA overnight. Beads were washed and precipitants analysed by SDS-PAGE.

In Vitro Ub Assays

Elongation assays: *In vitro* ubiquitination reactions were carried out in 1× ubiquitination buffer (50 mM Tris pH 7.4, 2.5 mM $MgCl_2$, 0.5 mM DTT) with the addition of 2 mM ATP, 0.5 μM Ube1, 0.7 μM 2W, 0.3–1 μM Ube2N/Ube2V2, 4 μg Ub and 1 μM E3. Reaction mixtures were incubated at 37°C for 1 hr, quenched by addition of LDS sample buffer and boiling at 95°C for 5 min.

Deubiquitination/degradation reactions: 10 μL 26S proteasome preparations were added to elongation assays after 1 hr ubiquitination reactions. Reaction mixtures were incubated at 37°C for 1 hr, quenched by addition of LDS sample buffer and boiling at 95°C for 5 min.

Single turnover E2∼Ub discharge assays: 40 μM Ube2N(K92R) was incubated for 30 min at 37°C with 370 μM Ub, 1 μM Ube1, 3 mM ATP in discharge buffer (50 mM HEPES pH 7.5, 150 mM NaCl, 20 mM $MgCl_2$). Then, 2 μM Ube2N(K92R)∼Ub was mixed 2.5 μM Ube2V2 and 1.5 μM TRIM5 protein in discharge buffer, supplemented with 50 mM L-Lysine. Samples were taken at the indicated time intervals, mixed with LDS sample buffer and boiled for 20 s, then resolved by LDS-PAGE and observed by immunoblot using anti-Ube2N (BioRad, AHP974, 1:1,000)

Confocal Microscopy

TE671, CrFK and 293T cells were seeded on round coverslips, pre-coated with poly-D-lysine for 293T cells. Cells were fixed for 10 min in 4 % paraformaldehyde, permeabilised for 20 min with 0.1 % Triton-X 100 and blocked for 1 hr with 5 % BSA in phosphate buffered saline (PBS). Intracellular targets were stained with specific antibodies for 1-2 hr at room temperature in 5 % BSA/PBS, followed by incubation with Alexa Fluor conjugated secondary antibodies for 1-2 hr at room temperature in 5 % BSA/PBS in the dark. Nuclei were detected with Hoesct 33342 (Life Technologies), and coverslips were mounted using SlowFade Diamond Antifade Mountant (Life Technologies). Imaging acquisition was performed on a Zeiss 780 inverted microscope (Zeiss) using 40× or 63× Oil objectives, using the Zen 2011 software. Images were analysed using FIJI/ImageJ software. To quantify TRIM5 CB, CB-containing cells were counted in 8-10 fields of view, translated into percentage of cells counted, then multiplied by the total number of cells transfected.

Mouse Immunizations

13 weeks old C57BL/6 mice (*n = 10*) were immunised subcutaneously (s.c) with 100 μg Ub(GA)RB protein in PBS mixed with complete Freund's adjuvant followed by 3 rounds of s.c boosting with 50 μg protein mixed with incomplete Freund's adjuvant. Boosting was done at days 24, 46 and 84. Tail bleeds for ELISA analyses were collected ad days 34, 59. Mice were sacrificed at day 105 and Intracardiac blood was collected.

ELISA

96 well plates (Nunc) were coated overnight with 1 μg/ml of Ub(GA)RING-B-Box2 (RB), RB or Ub. Plates were blocked with 2% milk in PBS, 0.05% Tween 20 (MPBST). Polyclonal sera diluted 1:60,000 in MPBST was pre-absorbed against a RB-coated plate for 35 min. Serum was removed from the plates, further diluted to 1:300,000 with MPBST and incubated for 1 hr on fresh antigen-coated plates. Plates were washed with PBST. Bound antibodies were detected with goat anti-mouse IgG-HRP (Jackson Immunoresearch, 115-035-071).

SEC-MALLS

100 μL TRIM5 RING-B-Box2 and Ub(G75/76A)RING-B-Box2 proteins were injected at 10 mg/mL in and resolved on a GE Superdex 75 10/300 GL (GE Healthcare) analytical column equilibrated in 50 mM Tris, pH 8.0, 150 mM NaCl, 1 mM DTT, in line with multi-angle laser light scattering using a Wyatt HELEOS-II 18-angle photometer coupled to a Wyatt Optilab rEX differential refractometer (Wyatt Technology Corp). Molecular weight calibration was performed with Bovine serum albumin (BSA). Data were collected and analyzed using ASTRA software.

QUANTIFICATION AND STATISTICAL ANALYSIS

Statistical significance was determined by unpaired *t* tests, using Graphpad Prism 7 software. *P value*s less than 0.05 were considered statistically significant. It was assumed that both WT TRIM5 and Ub(GA)TRIM5 were equally visible to N-monoUb- and K63-Ub-specific antibodies in untreated cells, which we also demonstrated. Where unstated, *n* = number of experimental replicates represented by data shown.